

DEPARTMENT OF PHYSICS
UNIVERSITY OF JYVÄSKYLÄ
RESEARCH REPORT No. 9/2001

NUCLEAR PARTON DISTRIBUTIONS: A PERTURBATIVE QCD ANALYSIS

BY
VESA KOLHINEN

Academic Dissertation
for the Degree of
Doctor of Philosophy



Jyväskylä, Finland
September 2001

URN:ISBN:978-951-39-9702-1
ISBN 978-951-39-9702-1 (PDF)
ISSN 0075-465X

Jyväskylän yliopisto, 2023

ISBN 951-39-1039-3
ISSN 0075-465X

DEPARTMENT OF PHYSICS,
UNIVERSITY OF JYVÄSKYLÄ
RESEARCH REPORT No. 9/2001

**NUCLEAR PARTON DISTRIBUTIONS:
A PERTURBATIVE QCD ANALYSIS**

**BY
VESA KOLHINEN**

Academic Dissertation
for the Degree of
Doctor of Philosophy

*To be presented, by permission of the
Faculty of Mathematics and Natural Sciences
of the University of Jyväskylä,
for public examination in Auditorium FYS-1 of the
University of Jyväskylä on October 5, 2001
at 12 o'clock noon*



Jyväskylä, Finland
September 2001

Preface

This work was carried out at the Department of Physics in the University of Jyväskylä during the years 1996-2001.

Most of all I express my gratitude to my two supervisors, doc. Kari J. Eskola and prof. Vesa Ruuskanen. I wish to thank Kari Eskola for his tireless guidance and supervision during these years. I also wish to thank Vesa Ruuskanen for initially introducing me to the world of particle and ultrarelativistic heavy ion physics, and offering me the possibility to study it further.

I am also grateful to the staff at the Department of Physics for providing an inspiring and pleasant working atmosphere.

I would like to thank all my friends both at the Department of Physics and in the real world, for their support and friendship. Although these people are too numerous to mention, I would like to name and thank Anniina Rytönen, Matias Aunola and Juhani Hämäläinen for their friendship and for all the unforgettable moments during all these years.

Finally, I wish to thank my family for everything.

Jyväskylä, September 2001

Vesa Kolhinen

Abstract

In this work the nuclear modifications of parton distributions are studied within the framework of perturbative QCD. It consists of four publications, of which the first two concentrate on the theoretical and numerical analysis of nuclear effects. In the last two articles further constraints for the nuclear effects are sought. This thesis follows the same structure: After a brief introduction in the chapter 1, the theoretical background for the processes in question is dealt in the chapter 2. In chapter 3, the analysis of nuclear effects is presented, and finally in the chapters 4 and 5 further constraints for the sea quark and gluon distributions are studied.

The nuclear effects are parametrized at the initial scale using only data from deep inelastic scattering and Drell-Yan experiments together with momentum and number density conservation as constraints [I]. QCD scale evolution of nuclear effects is studied using Dokshitzer-Gribov-Lipatov-Altarelli-Parisi (DGLAP) evolution equations. As a result, a scale dependent parametrization of nuclear effects is obtained for each parton flavour and nuclear mass number A [II].

The sea quark distribution is further studied in the Drell-Yan process in pA and Pb-Pb collisions in the region where the momentum fraction $x > 0.2$ [III]. In this region no direct experimental constraints for the parametrization are available; parametrization is fixed by the momentum conservation together with assumption of stable evolution. By considering different scenarios for the sea quark modifications in the region $x > 0.2$, we find that in Pb-Pb collisions at the SPS the effects of the order of 20 % could be seen at large M .

Finally, the lepton pairs produced via heavy mesons in pA collisions are studied at different energies in order to find out to what extent they could be used to further restrict the nuclear gluon modifications [IV]. The dominant process for heavy meson production in pA collision is $gg \rightarrow QQ$. As the mesons decay to leptons, the lepton pair cross section will thus reflect the properties of the gluon distribution. The results indicate that the ratios of lepton pair cross sections agree well with the nuclear modifications for gluons. Thus, sufficiently accurate measurements at different collider energies could be used to improve the accuracy of nuclear gluon distributions over a larger kinematical range.

List of publications

- [I] K.J. Eskola, V.J. Kolhinen and P.V. Ruuskanen: Scale evolution of nuclear parton distributions, Nucl. Phys. **B535** (1998) 351.
[https://doi.org/10.1016/S0550-3213\(98\)00589-6](https://doi.org/10.1016/S0550-3213(98)00589-6)
- [II] K.J. Eskola, V.J. Kolhinen and C.A. Salgado: The scale dependent nuclear effects in parton distributions for practical applications, Eur. Phys. J. C **9** (1999) 61.
<https://doi.org/10.1007/s100529900005>
- [III] K.J. Eskola, V.J. Kolhinen, C.A. Salgado and R.L. Thews: Constraints for the nuclear sea quark distributions from the Drell-Yan process at the SPS, JYFL-4/00, LPT Orsay 00-73, hep-ph/0009251, accepted to Eur. Phys. J. C.
<https://doi.org/10.1007/s100520100771>
- [IV] K.J. Eskola, V.J. Kolhinen and R. Vogt: Obtaining the nuclear gluon distribution from heavy quark decays to lepton pairs in pA collisions, JYFL-6/01, hep-ph/0104124, accepted to Nucl. Phys. A.
[https://doi.org/10.1016/S0375-9474\(01\)01221-0](https://doi.org/10.1016/S0375-9474(01)01221-0)

Author's contribution

The author has participated in the formulation of the problem and the preparation of the article [I], and also written an independent computer code confirming the results in publication.

The author has participated in the formulation and the preparation of the article [II]. The author has also participated in the numerical analysis of the results and helped to implement the obtained parametrization for nuclear effects (EKS98) into the CERN PDFLIB library.

The author has participated in the analysis of the problem and the preparation of the article [III] and has performed the numerical computations needed. The lowest order computations were done independently by CS, the NLO computations were done by the author only.

The author has participated in the formulation and the preparation of the article [IV], written the computer code used and performed all but NLO computations, and written the draft version of the article.

Contents

1	Introduction	1
1.1	Parton distributions	1
1.2	Nuclear parton distributions	2
2	Introduction to the processes	6
2.1	Deep inelastic scattering	6
2.1.1	Lowest order deep inelastic scattering .	6
2.1.2	Parton model	9
2.1.3	QCD improved parton model	11
2.2	Scale evolution .	13
2.3	Drell-Yan process	15
3	Nuclear effects	19
3.1	Parametrization of nuclear effects	19
4	Further constraints for sea quark distributions?	29
5	Further constraints for gluon distributions?	32
5.1	Lepton pair production	32
5.2	Correlated v. uncorrelated pairs .	36
5.3	Numerical calculations	37
5.4	Ratio of lepton pair cross sections	38
6	Conclusions	40
A	EKS98 parametrization	42

Chapter 1

Introduction

1.1 Parton distributions

Quantum chromodynamics (QCD) is a theory which describes the interactions of the elementary building blocks of matter, quarks and gluons, often referred also as partons. In the nature quarks are confined; they are bound together by gluons into hadrons. On the parton level the perturbative QCD (pQCD) predicts well the behaviour of the interacting partons in the perturbative region $Q \gg \Lambda_{\text{QCD}}$. On the hadronic level, for example in deep inelastic scattering (DIS) or in proton-proton collision the situation becomes more complicated as the structure of the hadron has to be taken into account. Since the partons interact with each other inside the hadron their exact momenta can not be determined. The probability of finding a parton with a given momentum fraction of the hadron's original momentum is described by number density distribution of the parton, or the *parton distribution* for short. In principle QCD describes the behaviour of the parton distributions but the calculations become too complicated to be performed. Thus the information of parton distributions must be obtained experimentally. Based on the measurements, several parametrizations of the parton distributions have been published by various groups (eg. [11]-[14]).

Generally, the parton distribution functions f_i , where i stands for a parton, $i = g, u, \bar{u}, d, \bar{d}, \dots$, depend on the momentum fraction x of nucleon's momentum carried by the parton, and the interaction energy scale Q^2 , $f_i = f_i(x, Q^2)$. They are universal in the sense that once they are determined at certain values of x and Q^2 for some process, they apply to all processes at the same x and Q^2 . For example, the cross sections for hard nucleon-nucleon

scatterings at high energies can be computed through factorization as

$$d\sigma(Q^2, \sqrt{s}) = \sum_{ij} f_i(x_1, Q^2) \otimes f_j(x_2, Q^2) \otimes d\hat{\sigma}_{ij}(Q^2, x_1, x_2) + \mathcal{O}\left(\frac{1}{Q^2}\right), \quad (1.1)$$

where $\hat{\sigma}_{ij}$ is a perturbatively calculable cross section for a specific partonic process and f_i is the parton distribution of the parton i . Usually these parton distributions are given for a free proton. The equivalent distributions for free neutrons are obtained by using the isospin symmetry.

1.2 Nuclear parton distributions

The parton distributions of nucleons which are bound to nuclei are different from those of the free ones. This has been observed in the measurements of the structure functions F_2^A in deep inelastic lepton-nucleus scatterings for a large number of nuclei [32]. The structure function F_2 is one of the structure functions which describe the properties of a hadron. In the parton model it can be expressed in terms of parton distributions; in the lowest order the relation is

$$F_2(x, Q^2) = \sum_q e_q^2 x (f_q(x, Q^2) + f_{\bar{q}}(x, Q^2)), \quad (1.2)$$

where e_q is the charge of the quark. The experimental results show that the ratio of F_2^A to the structure function of deuterium, F_2^A/F_2^D , differs from unity. As deuterium can to a good approximation considered as a sum of a free proton and a free neutron, this indicates that parton distributions of bound nucleons are different from those of free ones, $f_i^A(x, Q^2) \neq f_i(x, Q^2)$. Then for exaple the cross section for hard scattering at high energy nuclear collisions becomes

$$d\sigma(Q^2, \sqrt{s})_{AB} = \sum_{i,j=q,\bar{q},g} \left[Z_A f_i^{p/A}(x_1, Q^2) + (A - Z_A) f_i^{n/A}(x_1, Q^2) \right] \otimes \quad (1.3)$$

$$\otimes \left[Z_B f_j^{p/B}(x_2, Q^2) + (B - Z_B) f_j^{n/B}(x_2, Q^2) \right] \otimes d\hat{\sigma}(Q^2, x_1, x_2)_{ij} + \mathcal{O}\left(\frac{1}{Q^2}\right),$$

where $f_i^{p/A}$ stands for the parton distribution of parton type i in a proton in a nucleus A and Z_A stands for proton number of nucleus A .

The x dependence of the ratio $R_{F_2}^A \equiv F_2^A/F_2^D$ was observed already in the early measurements [15]. The Q^2 scale dependence of the ratio is much weaker, and thus it was observed much later. It was first detected in the measurements by the New Muon Collaboration (NMC) of the structure function F_2 of tin v. that of carbon, $F_2^{\text{Sn}}/F_2^{\text{C}}$ at small values of x [16]. An example of the data is shown in Fig. (1.1).

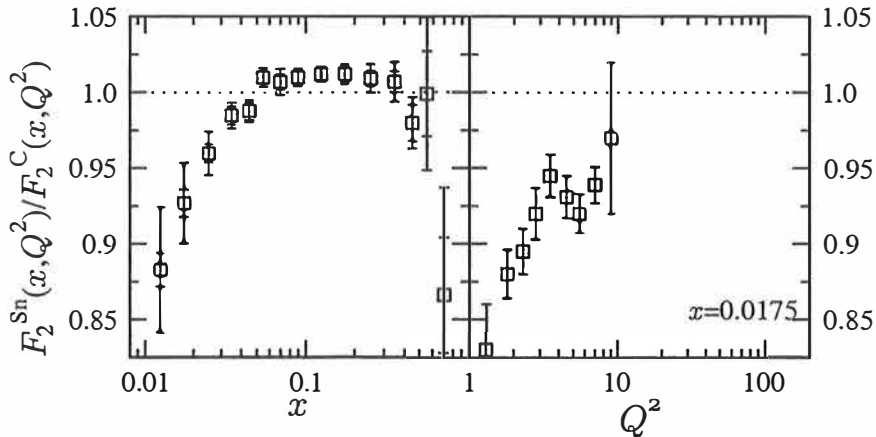


Figure 1.1: The ratio $F_2^{Sn}(x, Q^2)/F_2^C(x, Q^2)$ as a function of x (left panel) at different values of Q^2 [17], and as a function of Q^2 (right panel) at fixed $x = 0.0175$ [16].

The x dependence of $R_{F_2}^A$ is usually divided into four different regions: shadowing ($R_{F_2}^A \leq 1$) at $x \lesssim 0.1$, anti-shadowing ($R_{F_2}^A \geq 1$) at $0.1 \lesssim x \lesssim 0.3$, EMC effect ($R_{F_2}^A \leq 1$) at $0.3 \lesssim x \lesssim 0.7$ and Fermi motion ($R_{F_2}^A \geq 1$) at $x \rightarrow 1$ and beyond (Fig. (1.1)). At the moment the origin of these effects can not be explained by a single theoretical description. It is believed that different mechanisms are responsible for them in different kinematical regions.

Nuclear modifications in parton distributions play a role in all hard inclusive nuclear processes. Thus their contribution has to be taken into account in the calculations. Especially this is important for the inclusive cross sections of perturbative, hard processes, which are used as a reference in the search of the signals of quark gluon plasma (QGP). For example the amount of J/Ψ production, which is often used as this kind of signal, depends on the nuclear modifications in two different ways: First, the J/Ψ production is proportional to the nuclear gluon distributions. Second, the observed height of the J/Ψ peak depends on the normalization of the background events, which is fixed by fitting theoretical Drell-Yan results to the data. Again, the nuclear modifications appear in proton-nucleus or nucleus-nucleus Drell-Yan scattering.

In addition the calculations of the evolution of QGP requires an estimate of the initial condition [54, 55], and since QGP is produced in high energy nucleus-nucleus collisions, this estimate depends on the modifications of the parton distributions. Omission of nuclear effects in the theoretical calculations affect significantly the results and makes them less reliable.

Several models on the nuclear shadowing effects have been published. Models such as the vector meson dominance (VMD) [38, 39], the recombination model [28, 35, 37], pomeron exchange [40, 41] and pomeron exchange and VMD model combined [42, 43] attempt to describe the origin of the nuclear effects in hadronic processes. Generally they match the recent data qualitatively, but do not predict the results quantitatively. The vector meson dominance is based on an assumption that the interacting photon in fact fluctuates between a bare photon and a set of electromagnetic (e^+e^-) and hadronic states (vector mesons). In a parton fusion model partons from different nucleons overlap, causing interactions between them. The pomeron exchange model assumes that at small x the behaviour of F_2 is controlled by pomeron exchange, and the scattering photon probes essentially the parton content of the pomeron instead of that of the nucleus. An overview of the existing data and different models is given in Ref. [32].

Nuclear effects of parton distributions have also been studied in a model independent manner, using only the experimental data to parametrize them (e.g. [36]). This has also been the approach in this work. Our main goal has been to obtain expressions for the nuclear modifications of parton distributions, and to study whether the observed effects in $R_{F_2}^A$ can be explained by the pQCD scale evolution. In this analysis we have assumed that the nuclear effects factorize from the nuclear parton distributions, and that the scale evolution of nuclear parton distributions is similar to those of a free proton. This can be shown [27, 28] to apply in the approximation where $\sim 1/Q^2$ corrections are neglected.

When determining the scale dependent parton distributions, one of the main difficulties arises from the fact that experimental data from both DIS and proton-nucleus Drell-Yan (DY) experiments do not lie at fixed values of Q^2 , as would be ideal for the parametrization of the initial conditions for nuclear distributions (Fig 1.2). Thus, an iterative analysis is needed to constrain the parametrization: Starting at initial scale $Q^2 = Q_0^2 \gg \Lambda_{QCD}$, the parametrization for the nuclear distributions is evolved up to higher values of Q^2 using the Dokshitzer-Gribov-Lipatov-Altarelli-Parisi (DGLAP) [44, 45, 46] evolution equations of perturbative QCD. The results are then compared to data at corresponding Q^2 , and the initial parametrization is modified accordingly. As a result, a model independent parametrization is obtained for ratios $R_i^A(x, Q^2) \equiv f_i^A(x, Q^2)/f_i(x, Q^2)$, as a function of x , Q^2 , mass number A and parton flavour i [I, II].

We have also studied various possibilities to determine the nuclear sea [III] and gluon distributions [IV] more accurately. Currently the gluon distribution is constrained mainly by the momentum conservation and the sea quark distributions are fixed by the data only at low x . We find that with

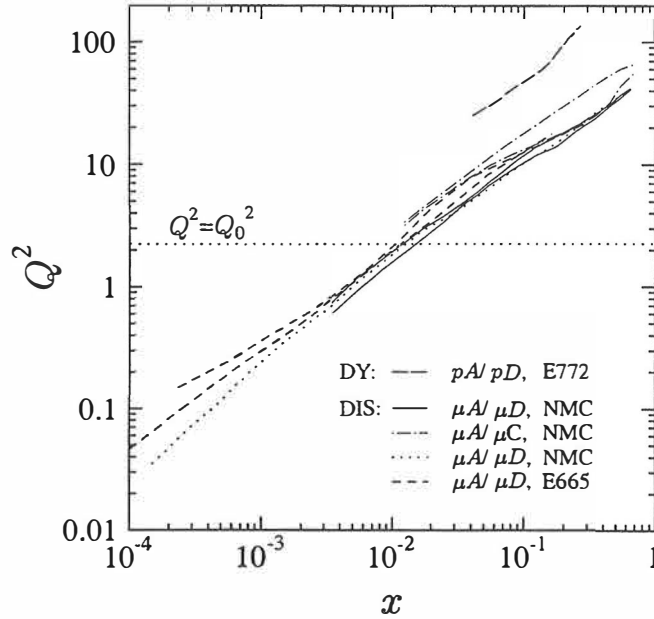


Figure 1.2: Correlation of the scale $\langle Q^2 \rangle$ and x in the measurements of $F_2^A(x, Q^2)$ in deeply inelastic IA and correlation of the invariant mass $\langle Q^2 \rangle$ and $x = x_2$ of Drell-Yan cross sections measured in pA collisions. The correlations in some of the NMC data [17] (solid lines), [19] (dotted-dashed), [18] (dotted) and in some of the E665 data [21] (dashed), and in the E772 data [25] (long dashed) are shown. The dotted line illustrates the chosen initial scale Q_0^2 , above which the DGLAP evolution is performed.

suitable experiments with sufficient accuracy the uncertainty in determining these distributions could indeed be reduced.

Chapter 2

Introduction to the processes

2.1 Deep inelastic scattering

Let us begin with a brief look at theoretical background of two of the processes which provide the most direct experimental information needed in this work, namely the deep inelastic scattering (DIS) and the Drell-Yan process (DY).

We will briefly outline how the structure functions enter into the cross sections and how they can be described using parton distribution functions of the parton model. We will then further expand the results using improved parton model, and finally see how the parton distributions are evolved with the interaction energy scale.

2.1.1 Lowest order deep inelastic scattering

The cross section of the scattering of a charged lepton from a hadron can be written as

$$\frac{d^2\sigma}{dE'd\Omega} = \frac{e^2}{16\pi^2Q^2} \frac{E'}{E} L_{\mu\nu} W^{\mu\nu}, \quad (2.1)$$

where

$$L_{\mu\nu} = \frac{1}{2} \text{Tr}(\not{k}'\gamma_\mu \not{k}\gamma_\nu) \quad (2.2)$$

is a leptonic tensor, and k (k') the four momentum of the incoming (outgoing) lepton. $W^{\mu\nu}$ is a hadronic tensor containing all the information of the interactions inside the hadron. In the most general case it is constructed out of metric tensor $g^{\mu\nu}$ and the independent four momenta of a hadron and a photon, p and q (see Fig. (2.1)). The requirements of symmetry and current conservation reduce the number of independent parameters in $W^{\mu\nu}$ to two,

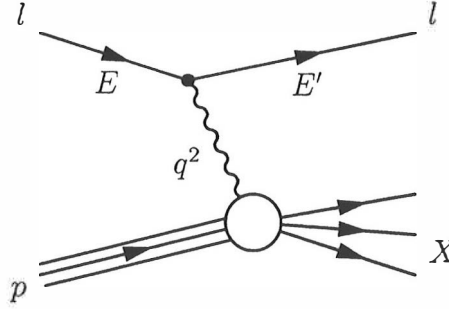


Figure 2.1: Lowest order deep inelastic lepton-proton scattering.

and $W^{\mu\nu}$ can be written as

$$W^{\mu\nu} = W_1(-g^{\mu\nu} - \frac{q^\mu q^\nu}{q^2}) + W_2 \frac{1}{M^2} (p^\mu - \frac{p \cdot q}{q^2} q^\mu)(p^\nu - \frac{p \cdot q}{q^2} q^\nu), \quad (2.3)$$

where W_1 and W_2 are Lorentz-invariant functions to be defined. In general they are functions of ν and Q^2 where $Q^2 = -q^2$,

$$q = k - k' \quad (2.4)$$

is the four momentum transfer and

$$\nu = E - E' \quad (2.5)$$

is the energy loss of the lepton.

Let us further define some variables needed later. In the laboratory frame and omitting the mass of a lepton, one obtains

$$Q^2 \equiv -q^2 = 4EE' \sin^2 \frac{\theta_{lab}}{2}, \quad (2.6)$$

$$x \equiv \frac{-q^2}{2p \cdot q} = \frac{Q^2}{2M\nu}, \quad (2.7)$$

$$y \equiv \frac{p \cdot q}{2p \cdot k} = \frac{\nu}{E} = 1 - \frac{E'}{E}. \quad (2.8)$$

In the laboratory frame the differential cross section can be written as

$$\frac{d^2\sigma}{dE d\Omega} = \frac{4\alpha^2 E'^2}{Q^2} \left[2W_1(\nu, Q^2) \sin^2\left(\frac{\theta_{lab}}{2}\right) + W_2(\nu, Q^2) \cos^2\left(\frac{\theta_{lab}}{2}\right) \right]. \quad (2.9)$$

For pointlike particles one can write

$$W_2 = \delta\left(\nu - \frac{Q^2}{2M}\right) = \frac{1}{\nu} \delta(1-x), \quad (2.10)$$

$$2W_1 = \frac{Q^2}{2M^2} \delta\left(\nu - \frac{Q^2}{2M}\right) = \frac{x}{M} \delta(1-x), \quad (2.11)$$

where one sees that the terms MW_1 and νW_2 for pointlike charges do not depend on ν and Q^2 separately, but only on $x = Q^2/(2M\nu)$. This is so called *Bjorken scaling*. It is characteristic for the lowest order calculations and arises from the fact that nucleons consist of pointlike partons. The scaling breaks down for the next to leading order calculations, because of the interaction between the partons.

Defining the structure functions F_1 and F_2 as

$$F_1(x, Q^2) = MW_1, \quad (2.12)$$

$$F_2(x, Q^2) = \nu W_2, \quad (2.13)$$

one obtains an expression for the differential cross section,

$$\frac{d^2\sigma}{dQ^2 dx} = \frac{4\pi\alpha^2}{Q^4} \frac{1}{x} \left[F_1(x, Q^2)xy^2 + F_2(x, Q^2)(1 - y - \frac{xy}{2} \frac{M}{E}) \right]. \quad (2.14)$$

The structure functions W_1 and W_2 are related to absorption of a virtual photon. For later discussion it is practical to express Eq. (2.14) using the total cross sections for absorption of longitudinal and transverse photons. The cross section for the absorption of a virtual photon with helicity λ is given by

$$\sigma_\lambda(\gamma^* N) = \frac{4\pi^2\alpha}{q_{lab}} \epsilon_\mu(\lambda) \epsilon_\nu^*(\lambda) W^{\mu\nu}. \quad (2.15)$$

For polarization vectors equation $\epsilon \cdot q = \epsilon^* \cdot q = 0$ hold. In addition, using Feynman gauge sets $\sum_\lambda \epsilon_\mu(\lambda) \epsilon_\nu^*(\lambda) \rightarrow -g_{\mu\nu}$. A convenient way to calculate the longitudinal cross section is by projection: the polarization vector can be written as a linear combination of p and q : $\epsilon_\mu(\lambda = 0) = ap_\mu + bq_\mu$. Using the properties of the polarization vectors, one obtains the expressions for the factors a and b . Then, in laboratory frame $(\epsilon(\lambda) \cdot p)(\epsilon^*(\lambda) \cdot p) = M^2(Q^2 + \nu^2)/Q^2$.

One can now define the longitudinal and transverse cross sections. The longitudinal total cross section turns out to be

$$\sigma_L(\gamma^* N) \equiv \sigma_{\lambda=0}(\gamma^* N) = \frac{4\pi^2\alpha}{\sqrt{\nu^2 + M^2}} \left[-W_1 + W_2 \left(1 + \frac{\nu^2}{Q^2} \right) \right], \quad (2.16)$$

and the transverse total cross section

$$\sigma_T(\gamma^* N) \equiv \frac{1}{2}(\sigma_{\lambda=1}(\gamma^* N) + \sigma_{\lambda=-1}(\gamma^* N)) = \frac{4\pi^2\alpha}{\sqrt{\nu^2 + M^2}} W_1. \quad (2.17)$$

Eqs. (2.12) and (2.13) leads now to

$$F_1 = \frac{M\sqrt{\nu^2 + M^2}}{4\pi^2\alpha} \sigma_T, \quad (2.18)$$

$$F_2 = \frac{M\sqrt{\nu^2 + M^2}}{4\pi^2\alpha} \left(\frac{\nu}{M} \right) \frac{1}{1 + \nu^2/Q^2} (\sigma_L + \sigma_T), \quad (2.19)$$

and to ratio

$$\frac{F_1}{F_2} = \frac{\frac{2M^2x}{Q^2} + \frac{1}{2x}}{1 + \frac{\sigma_L}{\sigma_T}}. \quad (2.20)$$

Finally, one obtains an expression for differential cross section of lepton-nucleon deep inelastic scattering: Eq. (2.14) can be written as

$$\frac{d^2\sigma}{dQ^2 dx} = \frac{4\pi\alpha^2}{Q^2} \frac{F_2(x, Q^2)}{x} \left(1 - y - \frac{xy}{2} \frac{M}{E} + \frac{y^2}{2} \frac{1 + \frac{4M^2x^2}{Q^2}}{1 + R(x, Q^2)}\right), \quad (2.21)$$

where

$$R(x, Q^2) = \frac{\sigma_L(\gamma^*p)}{\sigma_T(\gamma^*p)} \quad (2.22)$$

is a measure of the virtuality of the photon. The similar equation can be written for a lepton-nucleus case, normalized per nucleon:

$$\frac{1}{A} \frac{d^2\sigma}{dQ^2 dx} = \frac{4\pi\alpha^2}{Q^2} \frac{1}{A} \frac{F_2^A(x, Q^2)}{x} \left(1 - y - \frac{xy}{2} \frac{M_A}{E} + \frac{y^2}{2} \frac{1 + \frac{4M_A^2x^2}{Q^2}}{1 + R^A(x, Q^2)}\right), \quad (2.23)$$

For a nucleon the momentum fraction $0 \leq x \leq 1$, whereas for a nucleus $0 \leq x \leq A$. For nucleus the tail $x > 1$ is diminishingly small, and can safely be neglected. In this work we have done so and taken $x \leq 1$ for nuclei too.

We will assume that in the case of nuclear collisions the virtuality $R^A(x, Q^2)$ does not depend on nuclear mass number A . Assumption is reasonable since several experiments have shown that $\langle R^A - R^D \rangle \approx 0$ [29, 30, 31]. Thus, all nuclear dependence in this equation is in the structure function F_2 . It is immediately seen that the ratio of two cross sections of DIS at the same energy will reflect the ratio of structure functions F_2 at these processes. This is one of the basic relations which provide us experimental information about nuclear parton distributions.

2.1.2 Parton model

If the energy of the lepton in lepton-hadron scattering is large enough, the lepton will begin to resolve the structure of a hadron and eventually the quarks and gluons inside it. In such a case the lepton-hadron scattering can be rewritten in terms of parton model: Lepton interacts with pointlike quark inside the hadron. The cross section is similar to lepton-lepton scattering except that now the momentum of the quark is unknown. It can be written in terms of the momentum of the hadron, $p = \xi P$, where p and P are the

momenta of the quark and the hadron, respectively, and $0 < \xi < 1$ is the fraction of the momentum carried by the quark. The quark tensor becomes now

$$W_q^{\mu\nu} = \frac{e_q^2}{M} \xi \delta(\xi - x) \left(-\frac{1}{2} (g^{\mu\nu} - \frac{q^\mu q^\nu}{q^2}) - \frac{\xi}{P \cdot q} (P^\mu - \frac{P \cdot q}{q^2} q^\mu) (P^\nu - \frac{P \cdot q}{q^2} q^\nu) \right). \quad (2.24)$$

In order to get the cross section for lepton-hadron scattering, one has to sum over all the quarks and integrate over the quark momenta

$$d\sigma^{\ell h} = \sum_{i=u,d,s,\dots} \int_0^1 d\xi f_i(\xi) d\hat{\sigma}^{\ell i}, \quad (2.25)$$

where $d\hat{\sigma}$ is the cross section of lepton-quark scattering and $f_i(\xi)d\xi$ is the number of quarks of type i in the interval $[\xi P, (\xi + d\xi)P]$. Functions $f_i(\xi)$ are thus *number density distributions of partons* or *parton distributions* for short.

The differential lepton-hadron cross section becomes then

$$d\sigma^{\ell h} = \frac{1}{2s} \frac{e^4}{Q^4} \frac{d^3 k'}{(2\pi)^3 2k'^0} L_{\mu\nu} 4\pi M W^{\mu\nu}, \quad (2.26)$$

where

$$\begin{aligned} W^{\mu\nu} &= \sum_i \int_0^1 \frac{d\xi}{\xi} f_i(\xi) W_q^{\mu\nu} \\ &= \sum_i e_{q_i}^2 \frac{f_i(x)}{2M} (g^{\mu\nu} - \frac{q^\mu q^\nu}{q^2}) + \sum_i e_{q_i}^2 \frac{x f_i(x)}{M(P \cdot q)} (P^\mu - \frac{P \cdot q}{q^2} q^\mu) (P^\nu - \frac{P \cdot q}{q^2} q^\nu). \end{aligned} \quad (2.27)$$

In the above derivation a delta function term $\delta(\xi - x)$ set the momentum fraction ξ carried by the parton equal to the invariant variable x . Conversely, this means that the virtual photon must have the right value of ξ in order to be absorbed by the quark with given momentum fraction x .

By comparing equations (2.3) and (2.27) one can now identify F_1 and F_2 in terms of parton distributions:

$$F_1(x, Q^2) = M W_1 = \sum_q \frac{e_q^2}{2} f_q(x), \quad (2.28)$$

$$F_2(x, Q^2) = \nu W_2 = \sum_q e_q^2 x f_q(x). \quad (2.29)$$

One also obtains so called *Callan-Gross equation* for spin- $\frac{1}{2}$ particles:
 $2x F_1(x, Q^2) = F_2(x, Q^2)$.

2.1.3 QCD improved parton model

The parton model result presented above is in the lowest order (LO) in terms of the strong coupling constant α_s . It can be further improved by considering the next to leading order (NLO) QCD corrections. These corrections can be divided into three categories: virtual gluon corrections, real gluon emissions and initial state gluons.

Taking the gluon corrections into consideration leads to calculation of integrals which diverge. These divergencies are handled using so called regularization procedure. Common methods are to use massive gluon scheme (MG) or dimensional regularization scheme (DR). In massive gluon scheme the gluon is assumed to have a finite mass, which is finally set to zero. In dimensional regularization scheme the calculations are done in $N = 4 - 2\epsilon$ dimensions and ϵ taken to the limit $\epsilon \rightarrow 0$ at the end.

The divergencies can be categorized according to their origin: Ultraviolet divergencies originate from the self-energy terms of the interaction and can be absorbed into the definition of a coupling constant. Infrared divergency means that the emitted gluon is soft, i.e. its energy $E \rightarrow 0$, whereas collinear singularity means that the emitted gluon has a momentum collinear to that of the emitting quark. How these singularities cancel depends on the regularization scheme chosen. In the following the main results are given using dimensional regularization scheme. In this scheme the soft singularities will be proportional to $1/\epsilon^2$ and they will cancel out. The collinear divergencies proportional to $1/\epsilon$ will remain, however, and must be included, factored, into the definition of parton distributions. This procedure is, however, not unique. Several conventions exist, $\overline{\text{MS}}$ and DIS factorization schemes being the most common ones.

The interaction term in the lowest order (LO) in $\mathcal{O}(\alpha)$ can be represented schematically as

$$|\mathcal{M}|^2 \sim \left(\begin{array}{c} \text{---} \gamma^* \\ \text{---} \text{---} \\ \text{---} q \end{array} \right) \left(\begin{array}{c} \text{---} \gamma^* \\ \text{---} \text{---} \\ \text{---} q \end{array} \right)^* \quad (2.30)$$

Adding the virtual gluon corrections brings along the terms

$$|\mathcal{M}|^2 \sim \left(\begin{array}{c} \text{---} \gamma^* \\ \text{---} \text{---} \\ \text{---} q \end{array} + \begin{array}{c} \text{---} \gamma^* \\ \text{---} \text{---} \\ \text{---} q \end{array} + \begin{array}{c} \text{---} \gamma^* \\ \text{---} \text{---} \\ \text{---} q \end{array} \right) \left(\begin{array}{c} \text{---} \gamma^* \\ \text{---} \text{---} \\ \text{---} q \end{array} \right)^* + c.c. \quad (2.31)$$

In the emission of real gluons a quark emits a gluon before or after it

interacts with a photon. Graphically the process can be presented as:

$$|\mathcal{M}|^2 \sim \left| \begin{array}{c} \text{Diagram 1} \\ + \\ \text{Diagram 2} \end{array} \right|^2 \quad (2.32)$$

In the case of initial state gluon hadron emits a gluon which splits into a quark-antiquark pair, and one of them interacts with incoming photon.

$$|\mathcal{M}|^2 \sim \left| \begin{array}{c} \text{Diagram 1} \\ + \\ \text{Diagram 2} \end{array} \right|^2 \quad (2.33)$$

More explicit calculations of these corrections are represented in Ref. [2]. First order gluon corrections in photon quark interaction are also presented in Ref. [5] in the case of Drell-Yan process.

In $N \neq 4$ dimensions the gauge coupling e_N carries dimensions. It is therefore convenient to introduce so called *dimensional regularization mass*, m_D , and to define the N -dimensional α_s using the 4-dimensional one with a dimensional regularization mass,

$$\alpha_{sN} = \frac{\alpha_s}{(m_D^2)^{N/2-2}}. \quad (2.34)$$

Summing virtual and real gluon corrections leads to an expression which contains $1/\epsilon$ singularities. A convenient method to handle this situation is to define so called *plus functions* (which in the mathematical sense are not functions but distributions):

$$\int_z^1 dx f(x) \left(\frac{1}{1-x} \right)_+ \equiv \int_z^1 dx \frac{f(x) - f(1)}{1-x} + f(1) \ln(1-z). \quad (2.35)$$

Let us also define *splitting functions*, which describe the probability that a given particle emits another with a certain fraction of the momentum of the original particle:

$$P_{q_i q_j}(z) = \frac{4}{3} \left[\frac{1+z}{(1-z)_+} + \frac{3}{2} \delta(1-z) \right], \quad (2.36)$$

$$P_{qg}(z) = \frac{1}{2} [z^2 + (1-z)^2], \quad (2.37)$$

$$P_{gq}(z) = \frac{4}{3} \left[\frac{z^2 + (1-z)^2}{z} \right], \quad (2.38)$$

$$P_{gg}(z) = 6 \left[\frac{z}{(1-z)_+} + \frac{1-z}{z} + z(1-z) + \frac{11 - \frac{2}{3}N_f}{12} \delta(1-z) \right] \quad (2.39)$$

For example, function $P_{q_i q_j}$, sometimes written also as $P_{q_j \rightarrow q_i g}$, describes the probability that a quark q_j emits a gluon and the remaining quark q_i continues with the fraction of z of the original momentum. Similarly, function P_{qg} , or $P_{g \rightarrow q \bar{q}}$, describes a probability that a gluon splits into a quark-antiquark pair, in which the quark has fraction z of gluons momentum.

Summing up all the α_s corrections together results, after somewhat lengthy calculations [5], an expression for F_2 :

$$\begin{aligned} \frac{1}{x} F_2(x, Q^2) &= \sum_q e_q^2 [f_q(x, Q^2) + f_{\bar{q}}(x, Q^2)] \\ &+ \alpha_s \sum_q e_q^2 \left[\int_x^1 \frac{d\xi}{\xi} (f_q(\xi, Q^2) + f_{\bar{q}}(\xi, Q^2)) (f_q^{\text{DIS}}(z) - f_q^{\text{scheme}}(z)) \right. \\ &\left. + 2 \int_x^1 \frac{d\xi}{\xi} f_g(\xi, Q^2) (f_g^{\text{DIS}}(z) - f_g^{\text{scheme}}(z)) \right], \end{aligned} \quad (2.40)$$

where $z \equiv x/\xi$ and the quark distributions have been defined as

$$\begin{aligned} f_q(x, Q^2) &= \int_x^1 \frac{d\xi}{\xi} f_{q0}(\xi) \left[\delta(1-z) + \frac{\alpha_s}{2\pi} P_{qq}(z) \ln \left(\frac{Q^2}{m_D^2} \right) + \alpha_s f_q^{\text{scheme}}(z) \right] \\ &+ \int_x^1 \frac{d\xi}{\xi} f_{g0}(\xi) \left[\frac{\alpha_s}{2\pi} P_{qg}(z) \ln \left(\frac{Q^2}{m_D^2} \right) + \alpha_s f_g^{\text{scheme}}(z) \right], \end{aligned} \quad (2.41)$$

and the antiquarks $f_{\bar{q}}$ in a same manner. These expressions contain several unphysical terms, such as the bare parton distributions f_{q0} , $f_{\bar{q}0}$ and f_{g0} , a scale mass m_D^2 and scheme dependent functions f_j^{DIS} and f_j^{scheme} .

Also the collinear poles $1/\epsilon$ still remain in the expressions for f_j^{DIS} and f_j^{scheme} . This means that the definition of parton distributions depends on the choice of the factorization scheme. However, once their value is known at certain scale, their behaviour as a function of the interaction scale can be predicted, as will be seen in the next section.

In the lowest order, and in the DIS scheme in NLO, Eq. (2.40) becomes

$$F_2(x, Q^2) = \sum_q e_q^2 x [f_q(x, Q^2) + f_{\bar{q}}(x, Q^2)], \quad (2.42)$$

as already mentioned in section 1.2.

2.2 Scale evolution

As pointed out at the end of the section 2.1.3, perturbative QCD (pQCD) does not predict the absolute values of parton distributions. However, once

their values are fixed at some initial scale Q_0^2 , pQCD gives the change of the distributions as a function of the scale Q^2 . This is so called scale evolution, often referred also as Altarelli-Parisi or DGLAP evolution, derived by Altarelli and Parisi [44], Gribov and Lipatov [45] and Dokshitzer [46].

Heuristic derivation of evolution is rather straightforward. Let us consider flavour non-singlet case, $f_q^{NS}(x, Q^2) = f_q(x, Q^2) - f_{\bar{q}}(x, Q^2)$. By integrating the quark contribution in Eq. (2.41) over quark distribution function $f_q(\xi)$ one can now identify for each quark flavour [6]

$$f_q^{NS}(x, Q^2) = f_q^{NS(0)}(x) + \frac{\alpha_s}{2\pi} \int_x^1 \frac{d\xi}{\xi} f_q^{NS}(\xi) \left(P_{qq}\left(\frac{x}{\xi}\right) \ln\left(\frac{\mu^2}{m_D^2}\right) + 2\pi f_q^{\text{scheme}}\left(\frac{x}{\xi}\right) \right). \quad (2.43)$$

It is customary to denote $t = \ln(Q^2/\mu^2)$, where μ is used for the factorization scale. The scale μ is arbitrary but should be close to the subprocess interaction energy. Differentiating over t gives the relation between the scale dependent parton distributions and initial scale parton distributions.

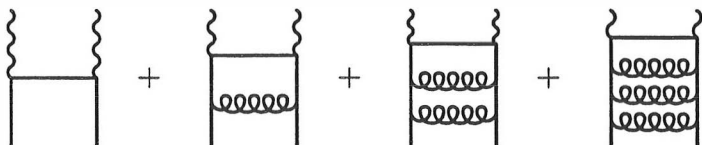
$$\frac{df_q^{NS}(x, t)}{dt} = \frac{\alpha_s}{2\pi} \int_x^1 \frac{d\xi}{\xi} f_q^{NS}(\xi, t) P_{qq}\left(\frac{x}{\xi}\right). \quad (2.44)$$

More general derivation for scale evolution can be performed using moment transformations, i.e. Mellin transformations, of the distributions.

The above derivation applies for non-singlet distributions only. More general expression for scale evolution which includes also gluon distributions, can be written in a matrix form:

$$\begin{aligned} \frac{d}{dt} \begin{pmatrix} f_q(x, t) \\ f_g(x, t) \end{pmatrix} & \quad (2.45) \\ &= \frac{\alpha_s(t)}{2\pi} \int_x^1 \frac{d\xi}{\xi} \begin{pmatrix} P_{qq}(x/\xi, \alpha_s(t)) & P_{qg}(x/\xi, \alpha_s(t)) \\ P_{gq}(x/\xi, \alpha_s(t)) & P_{gg}(x/\xi, \alpha_s(t)) \end{pmatrix} \begin{pmatrix} f_q(\xi, t) \\ f_g(\xi, t) \end{pmatrix}. \end{aligned}$$

These evolution equations sum the leading logarithm terms $(\alpha_s \ln(Q^2))^n$ of the interaction. The process can be expressed as summing the ladder graphs:



$$+ \dots \quad (2.46)$$

Functions P_{ij} are the splitting functions, and they form the evolution kernel of Altarelli-Parisi equations. They can be calculated as a power series

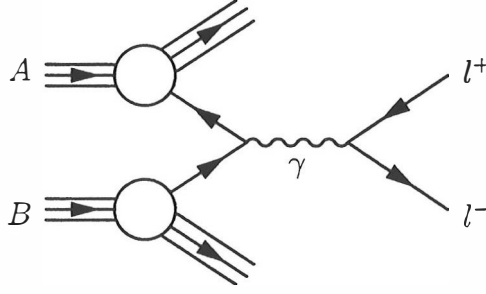


Figure 2.2: Lowest order Drell-Yan process in nucleus-nucleus collision.

of α_s . Denoting number of flavours by N_f , one can write down the first order estimate for them. This results the Eqs. (2.36)-(2.39).

DGLAP evolution will have an essential role in following chapters, where we determine the scale evolution and nuclear modifications for the parton distributions. Eq. (2.45) is practical for theoretical calculation but numerical evaluations requires more explicit form without any plus-functions. These expressions are given in next chapter, in Eqs. (3.11)-(3.13).

2.3 Drell-Yan process

Some of the data used for constraining the nuclear parton distribution in this work are provided by the Drell-Yan (DY) process in pA collisions. Let us therefore briefly present the cross section of this process expressed in terms of parton model, and see how the cross section reflects the parton distributions. The procedure is very much similar as in the case of deep inelastic scattering.

In the naive parton model the lowest order cross section of muon pair production in hadron-hadron collision is given by [3], [5]

$$\frac{d\sigma^{DY}}{dQ^2} = \frac{4\pi\alpha^2}{9Q^2s} \int_0^1 \frac{dx_1}{x_1} \frac{dx_2}{x_2} \left[\sum_q e_q^2 \left(f_q^{(1)}(x_1) f_{\bar{q}}^{(2)}(x_2) + f_q^{(2)}(x_2) f_{\bar{q}}^{(1)}(x_1) \right) \right] \times \delta\left(1 - \frac{\tau}{x_1 x_2}\right), \quad (2.47)$$

where Q is the mass of the lepton pair (often denoted also as M), and x_1 and x_2 are the momentum fractions of hadron carried by the quark and antiquark. Dimensionless variables are defined as

$$s = (p_A + p_B)^2, \quad (2.48)$$

$$\tau = \frac{Q^2}{s}, \quad (2.49)$$

and for the subprocess $\hat{s} = (p_q + p_{\bar{q}})^2 = 2p_q \cdot p_{\bar{q}}$.

Let us also define some kinematical variables and conventions which are used later. In the centre of mass frame (*cms*) the four momenta of the incoming quarks can be written as

$$\begin{cases} p_1 = \frac{\sqrt{s}}{2} x_1 (1, \underline{0}, 1) \\ p_2 = \frac{\sqrt{s}}{2} x_2 (1, \underline{0}, -1) \end{cases} \quad (2.50)$$

It is customary to use kinematical variables, *Feynman variable* x_F and *rapidity* y , defined as:

$$x_F = \frac{2p_z^\gamma}{\sqrt{s}}, \quad y = \frac{1}{2} \ln \left(\frac{E^\gamma + p_z^\gamma}{E^\gamma - p_z^\gamma} \right). \quad (2.51)$$

The conservation of four momentum implies

$$\begin{cases} x_1 = \frac{Q}{\sqrt{s}} e^{+y} = \frac{1}{2} (\sqrt{x_F^2 + 4\tau} + x_F), \\ x_2 = \frac{Q}{\sqrt{s}} e^{-y} = \frac{1}{2} (\sqrt{x_F^2 + 4\tau} - x_F), \end{cases} \quad (2.52)$$

which leads to $x_F = x_1 - x_2$ and $Q^2 = x_1 x_2 s$.

The double differential cross section in LO, corresponding to Eq. (2.47), can be written as

$$\frac{d^2\sigma^{DY}}{dQ^2 dx_F} = \frac{4\pi\alpha^2}{9Q^2 s} \frac{1}{x_1 + x_2} \left[\sum_q e_q^2 \left(f_q^{(1)}(x_1) f_{\bar{q}}^{(2)}(x_2) + f_q^{(1)}(x_2) f_{\bar{q}}^{(2)}(x_1) \right) \right]. \quad (2.53)$$

Clearly, Eqs. (2.47) and (2.53) reveal that the ratio of DY cross sections will reflect the ratio of the sums of the parton distributions.

Although the next-to-leading order (NLO) calculation is not used in analysis of the nuclear parton distributions, the NLO cross sections are evaluated in Ref. [III]. Thus we will also write an expression for the NLO cross section for Drell-Yan process. As in the case of DIS, the NLO corrections can be divided into virtual and real gluon corrections, and initial gluon emission. On the parton level these corrections can be presented schematically in the same way as for DIS in the section 2.1.3. As before, they lead to terms which contain infrared and collinear singularities.

Using the $\overline{\text{MS}}$ scheme to define the parton distributions, we get an expression for the NLO cross section: Putting all the corrections together yields [3],[5]

$$\frac{d\sigma^{DY}}{dQ^2} = \frac{4\pi\alpha^2}{9Q^2 s} \int_0^1 \frac{dx_1}{x_1} \int_0^1 \frac{dx_2}{x_2} \sum_q e_q^2 \left\{ \left(f_q^{(1)}(x_1, Q^2) f_{\bar{q}}^{(2)}(x_2, Q^2) + \right. \right.$$

$$\begin{aligned}
& + (1 \leftrightarrow 2) \left[\delta(1-z) + \frac{\alpha_s}{2\pi} (f_q^{DY}(z) - 2f_q^{\overline{\text{MS}}}(z)) \right] \\
& + \left[(f_q^{(1)}(x_1, Q^2) + f_{\bar{q}}^{(1)}(x_1, Q^2)) f_g^{(2)}(x_2, Q^2) + (1 \leftrightarrow 2) \right] \\
& \times \left[\frac{\alpha_s}{2\pi} (f_g^{DY}(z) - f_g^{\overline{\text{MS}}}(z)) \right] \Big\}, \tag{2.54}
\end{aligned}$$

where $z = \tau/(x_1 x_2)$ and

$$\begin{aligned}
f_q^{DY}(z) - 2f_q^{\overline{\text{MS}}}(z) &= \tag{2.55} \\
&= \frac{4}{3} \left[4(1+z^2) \left(\frac{\ln(1-z)}{1-z} \right)_+ - 2 \frac{1+z^2}{1-z} \ln z + \left(\frac{2\pi^2}{3} - 8 \right) \delta(1-z) \right],
\end{aligned}$$

$$\begin{aligned}
f_g^{DY}(z) - f_g^{\overline{\text{MS}}}(z) &= \tag{2.56} \\
&= \frac{1}{2} \left[(z^2 + (1-z)^2) \ln \left(\frac{(1-z)^2}{z} \right) - \frac{7}{2} z^2 + 3z + \frac{1}{2} \right].
\end{aligned}$$

The plus functions are defined in Eq. (2.35) in section 2.1.3.

The expression for the double differential cross section is somewhat more complicated. For the sake of completeness we will present the result here, also in $\overline{\text{MS}}$ scheme [8] (see also [9],[10]). The total differential cross section can be divided into annihilation and Compton terms:

$$\frac{d^2\sigma}{dQ^2 dx_F} = \frac{d^2\sigma^A}{dQ^2 dx_F} + \frac{d^2\sigma^C}{dQ^2 dx_F}, \tag{2.57}$$

where the annihilation term is

$$\begin{aligned}
\frac{d^2\sigma^A}{dQ^2 dx_F} &= \frac{4\pi\alpha^2}{9Q^2 s} \sum_q e_q^2 \int_{x_1}^1 dt_1 \int_{x_2}^1 dt_2 \left[\frac{d^2\hat{\sigma}^{LO}}{dQ^2 dx_F} + \frac{d^2\hat{\sigma}^A}{dQ^2 dx_F} \right] \\
&\times \left[f_q^{(1)}(t_1, Q^2) f_{\bar{q}}^{(2)}(t_2, Q^2) + f_q^{(2)}(t_2, Q^2) f_{\bar{q}}^{(1)}(t_1, Q^2) \right], \tag{2.58}
\end{aligned}$$

and the Compton term

$$\begin{aligned}
\frac{d^2\sigma^C}{dQ^2 dx_F} &= \frac{4\pi\alpha^2}{9Q^2 s} \sum_q e_q^2 \int_{x_1}^1 dt_1 \int_{x_2}^1 dt_2 \frac{d^2\hat{\sigma}^C}{dQ^2 dx_F} \\
&\times \left[f_g^{(1)}(t_1, Q^2) (f_q^{(2)}(t_2, Q^2) + f_{\bar{q}}^{(2)}(t_2, Q^2)) + (1 \leftrightarrow 2) \right]. \tag{2.59}
\end{aligned}$$

The annihilation part contains both the leading and the next-to-leading order terms. The LO term is

$$\frac{d^2\hat{\sigma}^{LO}}{dQ^2 dx_F} = \frac{1}{x_1 + x_2} \delta(t_1 - x_1) \delta(t_2 - x_2). \tag{2.60}$$

The contribution from NLO annihilation graphs is

$$\begin{aligned}
\frac{d^2\hat{\sigma}^A}{dQ^2 dx_F} &= \frac{1}{2} \frac{4\alpha_s(Q^2)}{3\pi} \frac{\delta(t_1 - x_1)\delta(t_2 - x_2)}{x_1 + x_2} \left[-8 + \frac{1}{3}\pi^2 + \ln^2(1 - x_1) \right. \\
&\quad \left. + \ln^2(1 - x_2) + 2\text{Li}_2(x_1) + 2\text{Li}_2(x_2) + 2\ln\left(\frac{x_1}{1 - x_1}\right)\ln\left(\frac{x_2}{1 - x_2}\right) \right] \\
&+ \frac{1}{2} \frac{4\alpha_s(Q^2)}{3\pi} \frac{\delta(t_2 - x_2)}{x_1 + x_2} \left[\frac{t_1^2 + x_1^2}{t_1^2(t_1 - x_1)_+} \ln\left(\frac{(x_1 + x_2)(1 - x_2)}{x_2(t_1 + x_2)}\right) + \frac{1}{t_1} - \frac{x_1}{t_1^2} \right. \\
&\quad \left. - \frac{t_1^2 + x_1^2}{t_1^2(t_1 - x_1)} \ln\frac{x_1}{t_1} + \frac{t_1^2 + x_1^2}{t_1^2} \left[\frac{\ln(1 - x_1/t_1)}{t_1 - x_1} \right]_+ \right] + (1 \leftrightarrow 2) \\
&+ \frac{1}{2} \frac{4\alpha_s(Q^2)}{3\pi} \left[\frac{\tilde{G}^A(t_1, t_2)}{[(t_1 - x_1)(t_2 - x_2)]_+} + \tilde{H}^A(t_1, t_2) \right]. \tag{2.61}
\end{aligned}$$

The dilogarithm function $\text{Li}_2(x)$ is defined as $\text{Li}_2(x) = -\int_0^x dt \frac{\ln(1-t)}{t}$, and the functions \tilde{G}^A and \tilde{H}^A are given by

$$\tilde{G}^A(t_1, t_2) = \frac{(t_1 + t_2)(\tau^2 + (t_1 t_2)^2)}{(t_1 t_2)^2(t_1 + x_2)(t_2 + x_1)}, \tag{2.62}$$

$$\tilde{H}^A(t_1, t_2) = \frac{-2}{t_1 t_2(t_1 + t_2)}. \tag{2.63}$$

The contribution from the Compton graphs is

$$\begin{aligned}
\frac{d^2\hat{\sigma}^C}{dQ^2 dx_F} &= \frac{3}{16} \frac{4\alpha_s(Q^2)}{3\pi} \frac{\delta(t_2 - x_2)}{(x_1 + x_2)t_1^3} \left[x_1^2 + (t_1 - x_1)^2 \right] \\
&\quad \times \ln \frac{(x_1 + x_2)(1 - x_2)(t_1 - x_1)}{x_1 x_2(t_1 + x_2)} + t_1^2 \Big] \\
&+ \frac{3}{16} \frac{4\alpha_s(Q^2)}{3\pi} \left[\frac{\tilde{G}^C(t_1, t_2)}{(t_2 - x_2)_+} + \tilde{H}^C(t_1, t_2) \right], \tag{2.64}
\end{aligned}$$

with

$$\tilde{G}^C(t_1, t_2) = \frac{\tau^2 + (t_1 t_2 - \tau)^2}{t_1^3 t_2^2 (t_2 + x_1)}, \tag{2.65}$$

$$\tilde{H}^C(t_1, t_2) = \frac{1}{(t_1 t_2)^2 (t_1 + t_2)^2} [t_1(t_2 + x_1)(t_2 - x_2) + 2\tau(t_1 + t_2)]. \tag{2.66}$$

These results are used in the numerical code [10] applied in the Ref. [III].

Chapter 3

Nuclear effects

3.1 Parametrization of nuclear effects

In this chapter we will deal with the nuclear modifications to the parton distributions. Our main goal is to obtain expressions for the nuclear modifications for the parton distributions, i.e. the ratios of nuclear and free parton distributions, $R_f^A(x, Q^2) \equiv f^A(x, Q^2)/f(x, Q^2)$. Especially we try to find constraints for the nuclear gluon distribution. In the previous works in this subject [34, 35, 36] the gluon distributions for the nuclei have been almost unknown. The only direct constraint for them has been the momentum conservation.

In recent experiments ratio of $F_2^{\text{Sn}}/F_2^{\text{C}}$ has been measured by the NMC [16]. Our aim is also to study whether this experimentally observed ratio could be explained using the DGLAP analysis of parton distributions.

As a result, the nuclear effects of parton distributions have been analysed and scale dependent expressions for them have been produced [I]. These have further been parametrized for practical applications [II]. The analysis and the parametrization of the nuclear distributions are explained in detail in Refs. [I] and [II].

Let us begin with a deep inelastic scattering from a nucleus A with a proton number Z . As shown in Eq. (2.23), the nuclear effects in the LO DIS cross section factorize into the structure function F_2 . In order to find out the amount of the nuclear effects, we compare the F_2^A to F_2^{D} of deuterium. Deuterium can to a good approximation be considered as a free proton plus a free neutron, without any shadowing effects. This is a reasonable assumption since the shadowing corrections to $(F_2^p + F_2^n)/2$ of deuterium are shown to be of the order 1 % at $x \gtrsim 0.007$ [53]. The choice of deuterium as a reference nucleus eliminates also some of the isospin effects. If also the nucleus A is

isoscalar, the isospin effects cancel out and the ratio of cross sections reflects directly the nuclear effects in parton distributions.

Writing down the ratio of structure functions of DIS gives

$$R_{F_2}^A(x, Q^2) \equiv \frac{F_2^A(x, Q^2)}{F_2^D(x, Q^2)} \quad (3.1)$$

$$= \frac{[F_2^{p/A}(x, Q^2) + F_2^{n/A}(x, Q^2)] + (2Z/A - 1)[F_2^{p/A}(x, Q^2) - F_2^{n/A}(x, Q^2)]}{F_2^{p/D}(x, Q^2) + F_2^{n/D}(x, Q^2)}. \quad (3.2)$$

Let us now simplify notations and denote $u \equiv f_u(x, Q^2)$ for the known distribution of u quarks in a free proton, and $u^A \equiv f_u^{p/A}(x, Q^2)$ for the average u -quark distribution in a bound proton of a nucleus A , and similarly for other quark flavours. For isoscalar nuclei $d^{n/A} = u^A$ and $u^{n/A} = d^A$. We will assume that this is a good approximation for the non-isoscalar nuclei as well. Using the lowest order QCD improved parton model below charm mass threshold, Eq. (2.42) gives

$$R_{F_2}^A(x, Q^2) = \frac{5(u^A + \bar{u}^A + d^A + \bar{d}^A) + 4s^A + (\frac{2Z}{A} - 1)3(u^A + \bar{u}^A - d^A - \bar{d}^A)}{5(u + \bar{u} + d + \bar{d}) + 4s}. \quad (3.3)$$

To get further constraints for the ratios of nuclear parton distributions we use the data of Drell-Yan cross section in pA collisions. The expression for the lowest order cross section is given in Eq. (2.53). The ratio of the cross sections for pA and pD collisions can be written as

$$\begin{aligned} R_{DY}^A(x_2, Q^2) &\equiv \frac{\frac{1}{A} d\sigma_{DY}^{pA}/dx_2 dQ^2}{\frac{1}{2} d\sigma_{DY}^{pD}/dx_2 dQ^2} \\ &= \{4[u_1(\bar{u}_2^A + \bar{d}_2^A) + \bar{u}_1(u_2^A + d_2^A)] \\ &\quad + [d_1(\bar{d}_2^A + \bar{u}_2^A) + \bar{d}_1(d_2^A + u_2^A)] + 4s_1 s_2^A + \dots\} / N_{DY} \\ &\quad + (\frac{2Z}{A} - 1) \{4[u_1(\bar{u}_2^A - \bar{d}_2^A) + \bar{u}_1(u_2^A - d_2^A)] \\ &\quad + [d_1(\bar{d}_2^A - \bar{u}_2^A) + \bar{d}_1(d_2^A - u_2^A)]\} / N_{DY} \end{aligned} \quad (3.4)$$

where

$$N_{DY} = 4[u_1(\bar{u}_2 + \bar{d}_2) + \bar{u}_1(u_2 + d_2)] + [d_1(\bar{d}_2 + \bar{u}_2) + \bar{d}_1(d_2 + u_2)] + 4s_1 s_2 + \dots \quad (3.5)$$

and we have used the notation $q_i^{(A)} \equiv f_q^{(A)}(x_i, Q^2)$ for $i = 1, 2$ and $q = u, d, s, \dots$. The variable Q^2 is the invariant mass of the lepton pair. The target (projectile) momentum fraction is $x_2(x_1)$, and $x_1 = Q^2/(sx_2)$.

Let us define the nuclear valence quark distributions as $q_V^A \equiv q^A - q_s^A = q^A - \bar{q}^A$ and the ratios of nuclear v. free proton distributions as

$$R_{\bar{q}}^A(x, Q^2) \equiv \frac{\bar{q}^A(x, Q^2)}{\bar{q}(x, Q^2)}, \quad R_{q_V}^A(x, Q^2) \equiv \frac{q_V^A(x, Q^2)}{q_V(x, Q^2)}. \quad (3.6)$$

Similarly we define $R_{\bar{u}+\bar{d}}^A \equiv (\bar{u}^A + \bar{d}^A)/(\bar{u} + \bar{d})$, $R_{\bar{u}-\bar{d}}^A \equiv (\bar{u}^A - \bar{d}^A)/(\bar{u} - \bar{d})$, $R_{u_V-d_V}^A \equiv (u_V^A - d_V^A)/(u_V - d_V)$ and for gluons $R_g^A \equiv g^A/g$.

Using the notations introduced in Ref. [I] one can now write Eqs. (3.3) and (3.4) using the above ratios, multiplied with suitable combinations of free parton distributions. Terms $R_{\bar{u}-\bar{d}}^A$ and $R_{u_V-d_V}^A$ appear in non-isoscalar part only, so concentrating to the isoscalar nuclei reduces Eq. (3.3) to simpler form. Since the DIS data [16, 17, 19, 20] which are used as a constraint for the parametrization in this work, are approximately corrected for non-isoscalar effects, this assumption can be justified.

Some further assumptions are needed, since there still are three variables to be fixed with two equations. Thus, as a first approximation we take $R_s^A(x, Q_0^2) = R_{\bar{u}+\bar{d}}^A(x, Q_0^2)$, $R_{\bar{q}}^A(x, Q_0^2) = R_S^A(x, Q_0^2)$, and similarly for the valence quarks $R_{u_V}^A(x, Q_0^2) = R_{d_V}^A(x, Q_0^2) = R_V^A(x, Q_0^2)$. This approximation is needed only at the initial scale Q_0^2 , in determining the initial distributions for the DGLAP evolution. In one of the parton distribution function sets used in the analysis, GRV-LO [13], it is assumed that $\bar{u}(x, Q_0^2) \equiv \bar{d}(x, Q_0^2)$ and thus the corresponding nuclear effects also remain equal throughout the evolution. In another set used in the analysis, CTEQ-4L [12], this equality is not assumed.

The above assumptions lead to two equations, one for DIS and one for DY, at a fixed scale Q_0^2 :

$$R_{F_2}^A(x, Q_0^2) = A_V^{IS}(x, Q_0^2) R_V^A(x, Q_0^2) + [A_{ud}^{IS}(x, Q_0^2) + A_s(x, Q_0^2)] R_S^A(x, Q_0^2), \quad (3.7)$$

$$R_{DY}^A(x, Q_0^2) = B_V^{IS}(x_1, x, Q_0^2) R_V^A(x, Q_0^2) + [B_{ud}^{IS}(x_1, x, Q_0^2) + B_s(x_1, x, Q_0^2)] R_S^A(x, Q_0^2) \quad (3.8)$$

The coefficients A_V^{IS} , A_{ud}^{IS} , A_s , B_V^{IS} , B_{ud}^{IS} and B_s , defined as in Ref. [I], are known exactly but depend on the parametrization of the parton distribution set used for a free proton.

In the following we have chosen $Q_0^2 = 2.25 \text{ GeV}^2$, conveniently below the charm mass threshold but in the perturbative region. These two equations would fix $R_V^A(x, Q_0^2)$ and $R_S^A(x, Q_0^2)$, if only the data lied on a constant Q_0^2 . As this is not the case, the scale evolution is needed to fix the parameters iteratively. The outline of the process is following:

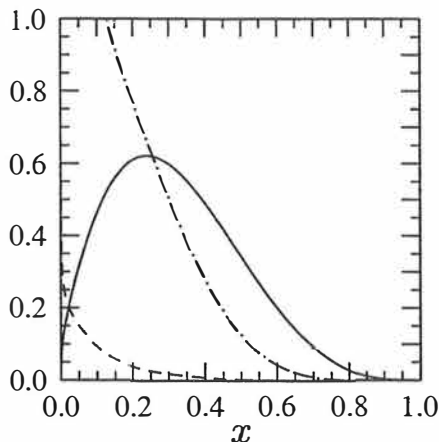


Figure 3.1: An example of typical parton distributions: xu_V (solid), $x\bar{u}$ (dashed) and xg (dotted-dashed) at $Q^2 = 2.25 \text{ GeV}^2$ for a free proton (MRST98 PDF set).

First, an initial parametrization is created for the ratio $R_{F_2}^A(x, Q_0^2)$. Second, $R_{F_2}^A(x, Q_0^2)$ is decomposed into $R_V^A(x, Q_0^2)$ and $R_S^A(x, Q_0^2)$. As a further constraint for nuclear valence quarks [36, 34], baryon number conservation

$$\int_0^1 dx [u_V(x, Q_0^2) + d_V(x, Q_0^2)] R_V^A(x, Q_0^2) = \int_0^1 dx [u_V(x, Q_0^2) + d_V(x, Q_0^2)] = 3 \quad (3.9)$$

is required.

At large values of x valence quarks dominate (see Fig. (3.1)) and $R_{F_2}^A$ follows R_V^A closely. In this region it is practically impossible to determine R_S^A directly from the data alone. Only momentum conservation and the requirement of a stable evolution can be used to constrain the sea quark ratio. At small x the situation is the opposite, sea quarks dominate and valence distributions are diminishingly small. To solve the problem, we used a piecewise construction to parametrize the ratios. At $x \lesssim 0.1$ R_V^A is fixed to have the same functional form as $R_{F_2}^A$ but with different parameters. This also fixes R_S^A in this region. At $0.1 < x \lesssim 0.4$ R_S^A is fixed simply by assuming a plateau in the ratio: $R_S^A(0.1 < x < 0.4, Q_0^2) = R_S^A(0.1, Q_0^2)$. This artificial plateau causes no significant physical effects and it disappears during evolution as R_S^A ratio smoothens.

At large x the ratios are set to be equal, $R_V^A(x, Q_0^2) = R_S^A(x, Q_0^2) = R_{F_2}^A(x, Q_0^2)$. Although the data and the momentum conservation do not show directly that there should be an EMC effect for sea quarks, one can conclude that there should be one. The EMC effect exists for the valence quarks and since the evolution of gluons is affected by the valence distributions, such an effect will be generated for gluons, too. As the evolutions of gluons and

sea quarks are coupled, an EMC like effect will also be generated for sea quarks. Thus, assuming that the evolution of the ratios is not very rapid at the beginning, it is plausible to assume an EMC effect both for the input gluon and sea quark distributions.

The gluon ratio $R_g^A(x, Q_0^2)$ is then estimated using momentum conservation and the behaviour of $R_g^A(x, Q_0^2)$ at small x . Since the sea quarks are shadowed at small x , we expect shadowing of the nuclear gluons as well. A requirement of stable scale evolution can be used together with the recent NMC data [16] to further constrain nuclear gluon shadowing. At the small x limit of the DGLAP equations one obtains

$$\begin{aligned} \frac{\partial R_{F_2}^A(x, Q^2)}{\partial \log Q^2} &= \frac{\partial F_2^D(x, Q^2)/\partial \log Q^2}{F_2^D(x, Q^2)} \left\{ \frac{\partial F_2^A(x, Q^2)/\partial \log Q^2}{\partial F_2^D(x, Q^2)/\partial \log Q^2} - R_{F_2}^A(x, Q^2) \right\} \\ &\approx \frac{5\alpha_s}{9\pi} \frac{2}{3} \frac{xg(2x, Q^2)}{F_2^D(x, Q^2)} \left\{ R_G^A(2x, Q^2) - R_{F_2}^A(x, Q^2) \right\}, \end{aligned} \quad (3.10)$$

where we have used the result¹ $\partial F_2(x, Q^2)/\partial \log Q^2 \approx 10\alpha_s xg(2x, Q^2)/(27\pi)$ [48]. Assuming similar saturation for the shadowing of gluons as for F_2^A , one can approximate $R_g(2x, Q^2) \approx R_g(x, Q^2)$ as $x \rightarrow 0$. Eq. (3.10) states, that as the factor $xg(2x, Q^2)/F_2^D(x, Q^2) > 0$, the derivative of R_{F_2} is such that R_{F_2} tends to R_g . A stable initial condition is thus obtained by requiring that $R_g(x, Q_0^2) \approx R_{F_2}(x, Q_0^2)$ at small values of x . If this approximation is assumed to be valid for all values of x , some momentum would be missing for all nuclei; for instance for $A = 208$ the depletion would be $\sim 11\%$. Thus, momentum conservation requires quite strong antishadowing for gluons. The functional form of R_G^A is given in Appendix of Ref. [I].

After the initial parametrization is created in the described manner, the parton distributions for all flavours are evolved to higher Q^2 using DGLAP evolution equations (2.45). In the evolution we neglected the parton fusion corrections, as we expect them to be small [36]. The HERA data [23, 24] shows no evidence of the fusion corrections at $Q^2 \gtrsim 1 \text{ GeV}^2$ and $x \gtrsim 10^{-4}$, and although the effect should be stronger in nuclei due to its expected $A^{1/3}$ scaling, we should still be in the safe region of x and Q^2 values.

The evolution itself is rather straightforward. Writing down Eqs. (2.45) in a numerically computable form one obtains:

$$\begin{aligned} Q^2 \frac{\partial xq_V^A(x, Q^2)}{\partial Q^2} &= \frac{\alpha_s(Q^2)}{\pi} \left\{ \frac{2}{3} \int_x^1 dy \frac{z}{y} \frac{(1+z^2)xq_V^A(y, Q^2) - 2xq_V^A(x, Q^2)}{1-z} \right. \\ &\quad \left. + \left(1 + \frac{4}{3} \ln(1-x)\right) xq_V^A(x, Q^2) \right\}, \end{aligned} \quad (3.11)$$

¹In the corresponding formulae in Ref. [I] factor 2/3 is missing.

$$\begin{aligned}
Q^2 \frac{\partial xq_s^A(x, Q^2)}{\partial Q^2} &= \frac{\alpha_s(Q^2)}{\pi} \left\{ \frac{2}{3} \int_x^1 dy \frac{z}{y} \frac{(1+z^2)xq_s^A(y, Q^2) - 2xq_s^A(x, Q^2)}{1-z} \right. \\
&+ \frac{1}{4} \int_x^1 dy \frac{z}{y} (z^2 + (1-z)^2) xg^A(y, Q^2) \\
&\left. + \left(1 + \frac{4}{3} \ln(1-x)\right) xq_s^A(x, Q^2) \right\}, \quad (3.12)
\end{aligned}$$

$$\begin{aligned}
Q^2 \frac{\partial xg^A(x, Q^2)}{\partial Q^2} &= \frac{\alpha_s(Q^2)}{\pi} \left\{ \frac{2}{3} \int_x^1 dy \frac{z}{y} \frac{1+(1-z)^2}{z} \right. \\
&\times \sum_{\substack{q=\text{all} \\ \text{flavours}}} x(q^A(x, Q^2) + \bar{q}^A(x, Q^2)) \\
&+ \frac{1}{2} \int_x^1 dy \frac{z}{y} 6 \left(\frac{zxg^A(y, Q^2) - xg^A(x, Q^2)}{1-z} + \right. \\
&+ \left. \left(\frac{1-z}{z} + z(1-z) \right) xg^A(y, Q^2) \right) \\
&\left. + \frac{1}{2} \left(\frac{11}{2} - \frac{1}{3} N_f + 6 \ln(1-x) \right) xg^A(x, Q^2) \right\}. \quad (3.13)
\end{aligned}$$

Here q_V^A ($q = u, d$) stands for nuclear valence and q_s^A ($q_s = u, \bar{u}, d, \bar{d}, s, \bar{s}, \dots$) for nuclear sea distributions. In addition $z = x/y$ and N_f is number of flavours. In our analysis $N_f = 3$ at the initial scale, and heavy quarks are generated by the evolution at their mass thresholds but treated as massless in the evolution.

In order to obtain the shadowing factors, the evolution equations (3.11)-(3.13) were solved numerically using two independent programs. Integrals were calculated using Fortran NAG libraries, and the differential equations were solved by using middle point trapezoidal formula (essentially 2nd order Runge-Kutta) and 4th order Runge-Kutta method [4]. The results were practically identical, which confirmed that the numerical evaluation was done adequately. The above analysis was performed using both GRV-LO [13] and CTEQ-4L [12] parametrizations for the free parton distributions, taken from CERN PDFLIB library [57] at the initial scale Q_0^2 .

The schematic picture of this procedure is shown in Fig. (3.2): The derivative of the parton distribution with respect to Q^2 at fixed value of x_i is obtained by evaluating the integrals from x_i to 1. Especially, the values of the distributions at $x < x_i$ do not contribute to the evolution at x_i .

The distributions were evolved from the initial scale $Q_0^2 = 2.25 \text{ GeV}^2$ up to $Q^2 = 10000 \text{ GeV}^2$. As the initial scale for CTEQ-4L is $Q_0^2 = 2.56 \text{ GeV}^2$, the distribution first had to be evolved downwards to 2.25 GeV^2 to

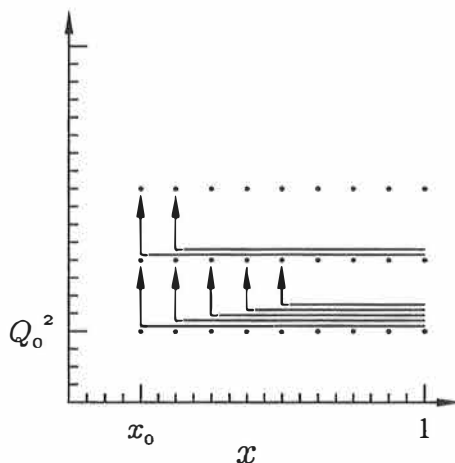


Figure 3.2: Schematic picture of the evolution: at fixed x_i the change of the distribution with respect to Q^2 is obtained by performing the integrals (3.11)-(3.13) from x_i to 1.

Experiment	x_{min}	x_{max}	Q_{min}^2 [GeV ²]	Q_{max}^2 [GeV ²]
NMC C (re)	0.0035	0.65	0.74	42
NMC Ca (re)	0.0035	0.65	0.60	41
NMC Sn/C	0.0125	0.7000	3.2	56.8
NMC Ca/C	0.0125	0.7000	3.4	66.4
NMC C (95)	0.00015	0.045	0.035	5.5
E665 Xe	0.00002	0.075	0.03	17.9
Re665	0.0002350	0.3087	0.1500	22.50
E772 C	0.041	0.269	25	138

Table 3.1: x and Q^2 regions probed at different experiments.

keep the analysis consistent. The evolved distributions were compared to the data and the initial conditions were modified accordingly. The process was repeated iteratively until the evolved distributions fit the data with an adequate accuracy. The data are shown in Fig. (1.2), and the x and Q^2 ranges of different experiments are also given in Table (3.1).

As a result, nuclear modifications for both GRV-LO and CTEQ-4L parametrizations were obtained. The ratios R_V^A , R_S^A , R_g^A and $R_{F_2}^A$ for an isoscalar nucleus $A = 208$ obtained using GRV-LO set are shown in Fig. (3.3).

Although the difference between the absolute parton distribution sets might be as large as ~ 2 for gluons, it turns out that in the ratios R_V^A , R_S^A , and R_g^A the set-dependence is quite small [II]. Since the expected difference

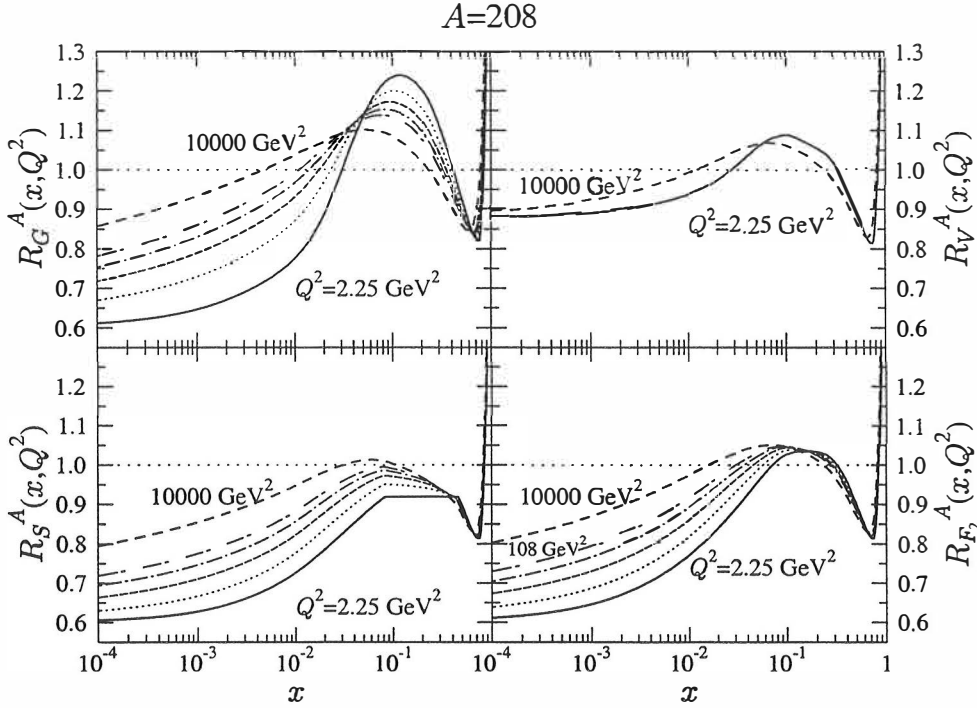


Figure 3.3: Scale evolution of the ratios $R_G^A(x, Q^2)$, $R_S^A(x, Q^2)$, $R_V^A(x, Q^2)$ and $R_{F_2}^A(x, Q^2)$ for an isoscalar nucleus $A=208$. The ratios are shown as functions of x at fixed values of $Q^2 = 2.25 \text{ GeV}^2$ (solid lines), 5.39 GeV^2 (dotted), 14.7 GeV^2 (dashed), 39.9 GeV^2 (dotted-dashed), 108 GeV^2 (double-dashed), equidistant in $\log Q^2$, and 10000 GeV^2 (dashed). For R_V^A only the first and last ones are shown. The ratios were obtained using GRV-LO [13] set for the free parton distributions.

between the sets is highest at large A and Q^2 , the calculated nuclear modifications were compared for $A = 208$ at $Q^2 = 10000 \text{ GeV}^2$. The results [II] show that the deviation of $R_i^{208}(x, Q^2)$ between the GRV-LO and CTEQ-4L sets is largest for gluons at small x , of the order of 5%. Comparing these to the uncertainties in determining the initial ratios, especially the shadowing at small x , and the behaviour of gluon distribution in general, one can conclude that the effect of set dependence can be neglected. The nuclear parton distribution for a parton type i in a nucleus A can thus be expressed by the terms of a corresponding free parton distribution and the obtained ratio R_i^A :

$$f_i^A(x, Q^2) = R_i^A(x, Q^2) f_i(x, Q^2). \quad (3.14)$$

The parton distributions are usually given for the free parton in a *proton*; Eq. (3.14) thus gives a parton distribution for a proton bound in a nucleus.

Assuming the isospin symmetry, the corresponding distributions can also be obtained in a bound neutron.

As the set dependence of parton distributions in the nuclear modifications appears to be small, it becomes appealing to provide a set independent parametrization for nuclear effects. The original modifications for nuclear effects were calculated using 180 values of $10^{-6} < x < 1$, 69 values of $2.25 \text{ GeV}^2 < Q^2 < 10^4 \text{ GeV}^2$, 8 values of A (4, 9, 12, 27, 40, 56, 117, 208) and for 8 types of parton flavour ($u_v, d_v, \bar{u}, \bar{d}, s, c, b, g$), making 794880 numbers in total. In order to make these nuclear modifications more useful for practical applications, a further parametrization of modifications was produced [II]. This parametrization, named as EKS98, is presented in detail in Appendix A. It provides nuclear modifications $R_i^A(x, Q^2)$ for the x and Q^2 regions mentioned above for each parton flavour and $A > 2$. It is also the first parametrization of the nuclear effects which has been included in the CERN PDFLIB library [57].

In Fig (3.4) the ratio $F_2^{\text{Sn}}/F_2^{\text{C}}$ is calculated in four different ways and compared to the data measured by the NMC [16]. Two of the curves are obtained directly using the nuclear ratios for GRV-LO [13] and CTEQ-4L [12] distributions separately, and two others are calculated by using the EKS98 [II] parametrization along with GRV-LO and CTEQ-4L free parton distributions. The difference between the curves is indeed insignificant.

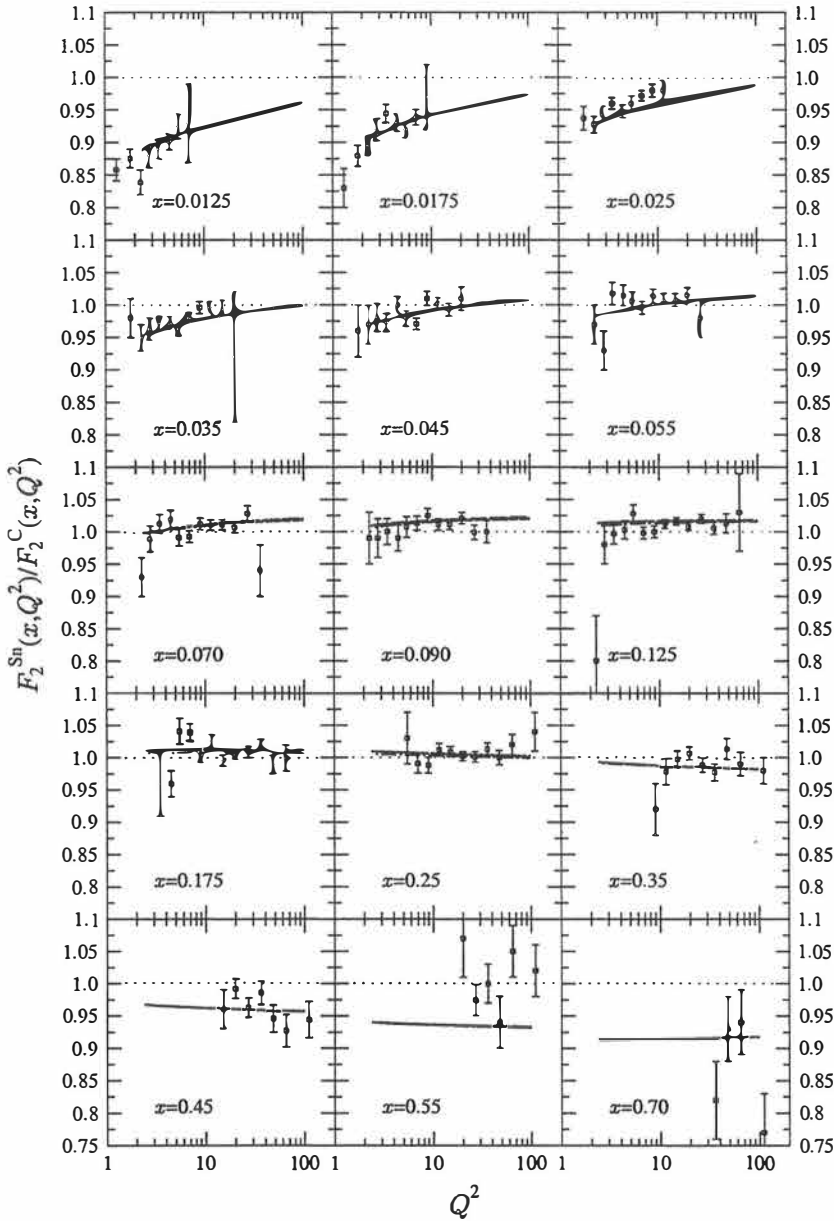


Figure 3.4: The ratio $F_2^{\text{Sn}}/F_2^{\text{C}}$ as a function of Q^2 at several different fixed values of x [16]. Two of the four curves in the figure are obtained directly using the nuclear ratios for the GRV-LO and CTEQ-4L distributions separately. Two other curves are calculated by using GRV-LO and CTEQ-4L distributions for free nucleons and taking nuclear effects from the EKS98 parametrization. As seen in the figure, the difference between the calculated curves is barely visible.

Chapter 4

Further constraints for sea quark distributions?

As pointed out in Chapter 3, valence quark distributions dominate the structure function F_2^A at large $x \gtrsim 0.2 \dots 0.3$. Therefore, the ratio $R_{F_2}^A$ effectively constrains the valence quark ratio R_V^A but not that of the sea quarks, R_S^A or gluons, R_g^A . Momentum conservation and the requirement of stable evolution are about the only methods to fix sea quark ratio at this region. As explained in Chapter 3, we have assumed an EMC effect for sea quark distributions. In order to improve the input distribution of the DGLAP analysis and to find additional experimental constraints for the nuclear modifications of sea quarks, we have studied the nuclear effects in Drell-Yan process at the SPS energies [III].

The nuclear effects in the Drell-Yan process can be divided into two categories. First there are effects arising from the dynamics of a collision. These can be described as the “genuine” nuclear effects and they also include the modifications of parton distributions. Second, the isospin effects, i.e. different relative proton and neutron numbers, cause difference between the isoscalar and non-isoscalar pA collisions even if the nuclear modifications on parton distributions or collision dynamics were neglected.

The ratio of the inclusive Drell-Yan cross section in pA v. pD collisions was given in Eq. (3.4). For isoscalar nuclei this ratio reflects directly the nuclear modifications of parton distributions. For non-isoscalar nuclei, however, the isospin effects have to be taken into account. It turns out that the isospin corrections are very sensitive for the parton distribution set chosen. In the earliest sets it was assumed that $\bar{u} = \bar{d}$. Measurements of NA51 Collaboration showed that this is not the case, but instead the ratio $\bar{u}/\bar{d} = 0.51 \pm 0.04 \pm 0.05$ at $x = 0.18$ [33]. In the study of the behaviour of the sea distributions, we have used modern parton distribution sets which take the $\bar{u} \neq \bar{d}$ asymmetry

into account.

We have calculated the cross sections $\frac{1}{A} \frac{d\sigma_{DY}^{pA}}{dM} / \frac{d\sigma_{DY}^{pp}}{dM}$ and $\frac{1}{A} \frac{d\sigma_{DY}^{pA}}{dM} / \frac{1}{2} \frac{d\sigma_{DY}^{pD}}{dM}$, which can be formed using the results of NA50 measurements at the CERN SPS. They have measured the inclusive dilepton production in pp, pD, p- ^9_4Be and p- $^{184}_{74}\text{W}$ collisions at $E_{\text{lab}} = 450 \text{ GeV}$ ($\sqrt{s} = 30 \text{ GeV}$), using the rapidity range $3 < y_{\text{lab}} < 4$ ($-0.46 < y_{\text{cm}} < 0.54$) and mass M around the J/Ψ peak. For $M \gtrsim 4 \text{ GeV}$, the mass spectrum is dominated by Drell-Yan dileptons.

We calculated the above ratios of cross sections using MRST98 (central gluon) parton distribution set [11] and integrating over the NA50 rapidity bin. Although the nuclear modifications $R_i^A(x, Q^2)$ are determined in the lowest order only, we calculated also the next to leading order cross sections. This can be justified because the Q^2 evolution of the nuclear modifications is slow. The EKS98 parametrization can thus be used as a first approximation for the NLO calculations as well. The results in Ref. [III] show that the LO and NLO results are very close to each other and the LO results are a good approximation to the NLO ones.

The net effect of nuclear modifications in Drell-Yan ratios turn out to be small at the SPS energy $E_{\text{lab}} = 450 \text{ GeV}/c$ and in the kinematical region $1 \text{ GeV} \lesssim M \lesssim 10 \text{ GeV}$, $3 < y_{\text{lab}} < 4$. This is mainly because of two reasons. First, the nuclear effects for sea quarks at the probed x_2 values are small, and second, the corresponding valence distribution is antishadowed in this region. These two effects partly cancel each others, leaving only a weak net effect. Thus, in this region the experimental measurements are not necessarily accurate enough to fix the nuclear modifications.

In an attempt to find constraints for nuclear sea distributions in the EMC region, one must consider larger values of x . This implies using lower energies. The NA50 Collaboration has measured the dilepton production also in Pb-Pb collisions at $E_{\text{lab}} = 158 \text{ AGeV}$ ($\sqrt{s} = 17.2 \text{ GeV}$). This data would provide useful constraints, if only there were data for pp or pD events at the corresponding energy. To our knowledge, however, no such data exist. In theory the ratio of Pb-Pb v. pp or pD cross sections could be formed using pp or pD data from different experiments, rescaled to the correct energy, or, by taking them directly from theoretical calculations.

We have studied the sensitivity of the Drell-Yan cross section to the different assumptions of the sea quark modifications in the EMC region. First we calculated the ratio of shadowed v. non-shadowed Drell-Yan cross sections, $\frac{d\sigma_{\text{shad}}^{\text{PbPb}}}{dM^2} / \frac{d\sigma_{\text{non-shad}}^{\text{PbPb}}}{dM^2}$, in a normal manner using the usual EKS98 nuclear modifications. Second, we used EKS98 for valence and also for sea at $x < 0.1$ but assumed no EMC effect for sea. Instead, we interpolated $R_S(x, Q^2)$ linearly from $x = 0.3$ to the region of Fermi motion, at $x \gtrsim 0.8$. Third, we set

$R_{\bar{q}} = 1$ and used no nuclear modifications for sea quarks at all. The results show (See Fig 5. in Ref. [III]) that using EKS98 the net nuclear effect in the ratio is of the order of 20 % at masses larger than 7 GeV. In this region the other scenarios give only ~ 10 % nuclear effects. At smaller mass values the ratios of different scenarios are closer to each other: the ones containing nuclear effects show some 5 % depletion at $M=3$ GeV, while the scenario with no nuclear effects for the sea quarks has practically no depletion at all at this M . We conclude, that if the measurements of the ratio of Drell-Yan cross sections at $E_{\text{lab}} = 158$ AGeV were made with a precision of ~ 5 -10 % or better, they could be used to constrain the EMC effect of nuclear sea quark distributions.

The effects of nuclear modifications in Drell-Yan process have further consequences as dileptons are used in determining the J/Ψ spectrum. Our study [III] shows that the slope of the invariant mass distribution of Drell-Yan pairs is affected by nuclear effects. At J/Ψ peak $M \sim 3$ GeV the nuclear shadowing effect is 5 %, whereas at $M \geq 7$ GeV it is 20 %, as pointed out above. However, the data at large mass values have smaller weight in the χ^2 fits because of large statistical uncertainties, and thus the fits are dominated by data around mass values of 4 GeV. The nuclear effects are therefore expected to remain smaller than 5 % for the extrapolation of Drell-Yan cross section from 4 GeV down to 3 GeV.

Chapter 5

Further constraints for gluon distributions?

As previously mentioned, the initial conditions for nuclear gluon distributions can be constrained only indirectly using the scale dependence of the ratio $F_2^A(x, Q^2)$. Unfortunately, the only measured set of data is the ratio $F_2^{\text{Sn}}/F_2^{\text{C}}$ at $0.02 < x < 0.2$ by the NMC [16]. At other values of x , gluon distribution can be restricted only by the requirement of stable evolution and the momentum conservation which provides an overall limit, essentially determining the amount of antishadowing of $R_g^A(x, Q_0^2)$. In order to find additional constraints for the nuclear gluon modifications at the initial scale, we have studied the heavy quark induced lepton pair production in pA collisions.

5.1 Lepton pair production

The dominant process which produces heavy quark pairs ($QQ = c\bar{c}, b\bar{b}$) in pA or pp collision is mediated via gluons: $gg \rightarrow QQ$. These quarks fragment into heavy mesons such as D or B , which may later decay semileptonically. The resulting lepton pairs therefore carry direct information of the input gluon distributions of the colliding hadrons. The ratio of lepton pair cross sections in pA and pp collisions, $d\sigma^{\text{p}A}/d\sigma^{\text{pp}}$, should thus reflect the nuclear modifications of gluons, $R_g^A(x, Q^2)$. To qualify this has been the main goal in Ref. [IV].

In order to study the R_g^A dependence of the ratio of cross sections, we have calculated the lepton pair cross sections in pA and pp collisions using the EKS98 parametrization of nuclear modifications [II] for bound nucleons.

The general picture of the process is described in Fig. (5.1). The corre-

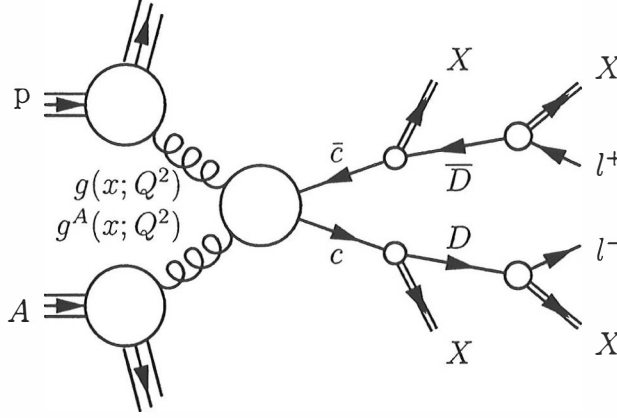


Figure 5.1: Lepton pair production in nucleon–nucleus collision. The most dominant process is mediated via gluons, which produce a $Q\bar{Q}$ pair. Quarks fragment into heavy mesons $H\bar{H}$, which may decay semileptonically.

sponding differential cross section of lepton pair production is

$$\begin{aligned} \frac{d\sigma^{\text{PA} \rightarrow \bar{l}l+X}}{dM_{\bar{l}l} dy_{\bar{l}l}} &= \int d^3\vec{p}_l d^3\vec{p}_{\bar{l}} \int d^3\vec{p}_H d^3\vec{p}_{\bar{H}} \delta(M_{\bar{l}l} - M(p_l, p_{\bar{l}})) \delta(y_{\bar{l}l} - y(p_l, p_{\bar{l}})) \\ &\times \frac{d\Gamma^{H \rightarrow l+X}(\vec{p}_H)}{d^3\vec{p}_l} \frac{d\Gamma^{\bar{H} \rightarrow \bar{l}+X}(\vec{p}_{\bar{H}})}{d^3\vec{p}_{\bar{l}}} \frac{d\sigma^{\text{PA} \rightarrow H\bar{H}+X}}{d^3\vec{p}_H d^3\vec{p}_{\bar{H}}} \\ &\times \theta(y_{\min} < y_l, y_{\bar{l}} < y_{\max}) \theta(\phi_{\min} < \phi_l, \phi_{\bar{l}} < \phi_{\max}) . \end{aligned} \quad (5.1)$$

where we have generically denoted the heavy quarks as Q and heavy meson as H , and where $M_{\bar{l}l}$ and $y_{\bar{l}l}$ are the invariant mass and the rapidity of the lepton pair, defined as

$$M(p_l, p_{\bar{l}}) = \sqrt{(p_l + p_{\bar{l}})^2} , \quad (5.2)$$

$$y(p_l, p_{\bar{l}}) = \frac{1}{2} \ln \left(\frac{(E_l + E_{\bar{l}}) + (p_{lz} + p_{\bar{l}z})}{(E_l + E_{\bar{l}}) - (p_{lz} + p_{\bar{l}z})} \right) . \quad (5.3)$$

The θ functions define the acceptance cuts in the detector simulations for the rapidity and azimuthal angle of a single lepton.

The produced mesons may decay semileptonically. The decay rate is denoted by $d\Gamma^{H \rightarrow l+X}(\vec{p}_H)/d^3\vec{p}_l$, and it gives the probability distribution that a meson H with momentum \vec{p}_H decays to a lepton l with momentum \vec{p}_l . Taking the integrated decay rate to leptons v. anything gives the branching ratio, $B \equiv \Gamma^l/\Gamma$, the probability that the meson produces a lepton. We have used values $B = 0.172$ for D^\pm and $B = 0.105$ for B^\pm decay to leptons.

Using a fragmentation function D_Q^H to describe quark fragmentation to mesons, the $H\bar{H}$ production cross section can be written as

$$\begin{aligned} \frac{d\sigma^{\text{pA} \rightarrow H\bar{H}+X}}{d^3\vec{p}_H d^3\vec{p}_{\bar{H}}} &= \int \frac{d^3\vec{p}_Q}{E_Q} \frac{d^3\vec{p}_{\bar{Q}}}{E_{\bar{Q}}} E_Q E_{\bar{Q}} \frac{d\sigma^{\text{pA} \rightarrow Q\bar{Q}+X}}{d^3\vec{p}_Q d^3\vec{p}_{\bar{Q}}} \\ &\times \int_0^1 dz_1 D_Q^H(z_1) \int_0^1 dz_2 D_{\bar{Q}}^{\bar{H}}(z_2) \delta^{(3)}(\vec{p}_H - z_1\vec{p}_Q) \delta^{(3)}(\vec{p}_{\bar{H}} - z_2\vec{p}_{\bar{Q}}) \end{aligned} \quad (5.4)$$

where z is the fraction of the parent quark momentum carried by the final state meson. There are several different models for fragmentation functions. In this work we have chosen the simplest one, the delta function fragmentation, $D_Q^H(z) = \delta(1 - z)$, which assumes that each quark will always produce one hadron. The results have also been confirmed using another typical fragmentation function, the Peterson *et al.* fragmentation [52], in which the meson momentum is smeared according to

$$D_Q^H(z) = \frac{N}{z(1 - (1/z) - \epsilon_Q/(1 - z))^2} \quad (5.5)$$

The normalization, N , is fixed by the requirement $\sum_H \int_0^1 dz D_Q^H(z) = 1$. The peak of the fragmentation function is at $z \approx 1 - 2\epsilon_Q$ with a width $\epsilon_Q \approx (m_q/m_Q)^2$. We have assumed e.g. that all the c quarks fragment into D mesons so that $H \equiv D$ for charm. In the ratio of pA v. pp cross sections the difference caused by different fragmentation schemes is negligible.

The hadronic heavy quark production cross section *per nucleon* in pA collisions can be factorized into the general form

$$\begin{aligned} \frac{1}{A} E_Q E_{\bar{Q}} \frac{d\sigma^{\text{pA} \rightarrow Q\bar{Q}+X}}{d^3\vec{p}_Q d^3\vec{p}_{\bar{Q}}} &= \sum_{i,j} \int_0^1 dx_1 \int_0^1 dx_2 f_i^p(x_1, Q^2) f_j^A(x_2, Q^2) E_Q E_{\bar{Q}} \\ &\times \frac{d\hat{\sigma}^{ij \rightarrow Q\bar{Q}}}{d^3\vec{p}_Q d^3\vec{p}_{\bar{Q}}} \end{aligned} \quad (5.6)$$

The parton distributions are evaluated at the scale $Q^2 \sim m_T^2 = p_T^2 + m_Q^2$. To lowest order, LO, the partonic cross section is

$$E_Q E_{\bar{Q}} \frac{d\hat{\sigma}^{ij \rightarrow Q\bar{Q}}}{d^3\vec{p}_Q d^3\vec{p}_{\bar{Q}}} = \frac{\hat{s}}{2\pi} \frac{d\hat{\sigma}^{ij \rightarrow Q\bar{Q}}}{d\hat{t}} \delta^{(4)}(p_1 + p_2 - p_Q - p_{\bar{Q}}), \quad (5.7)$$

where p_1 and p_2 are the four momenta of the incoming partons.

Finally, the cross sections for lowest order (LO) subprocesses for heavy quark pair production, convoluted with parton distributions can be written

as

$$\sum_{i,j} f_i^p(x_1, Q^2) f_j^A(x_2, Q^2) \frac{d\hat{\sigma}^{ij \rightarrow Q\bar{Q}}}{d\hat{t}} = \frac{1}{16\pi\hat{s}^2} \left(f_g^p(x_1, Q^2) f_g^A(x_2, Q^2) \overline{|\mathcal{M}_{gg \rightarrow Q\bar{Q}}|^2} \right. \\ \left. + \sum_{q=u,d,s} [f_q^p(x_1, Q^2) f_q^A(x_2, Q^2) + f_q^p(x_1, Q^2) f_q^A(x_2, Q^2)] \overline{|\mathcal{M}_{q\bar{q} \rightarrow Q\bar{Q}}|^2} \right). \quad (5.8)$$

When summed (averaged) over final (initial) state colours and spins, the squared matrix elements can be written as (see e.g. Ref. [51])

$$\sum |\overline{|\mathcal{M}_{gg \rightarrow Q\bar{Q}}|^2}|^2 = \frac{64}{9} \frac{\pi^2 \alpha_s^2}{\hat{s}^2} \{ (m^2 - \hat{t})^2 + (m^2 - \hat{u})^2 + 2m^2 \hat{s} \}, \quad (5.9)$$

and

$$\sum |\overline{|\mathcal{M}_{q\bar{q} \rightarrow Q\bar{Q}}|^2}|^2 = \quad (5.10) \\ \pi^2 \alpha_s^2 \left[\frac{12}{\hat{s}^2} (m^2 - \hat{t})(m^2 - \hat{u}) + \frac{8}{3} \frac{(m^2 - \hat{t})(m^2 - \hat{u}) - 2m^2(m^2 + \hat{t})}{(m^2 - \hat{t})^2} \right. \\ \left. + \frac{8}{3} \frac{(m^2 - \hat{t})(m^2 - \hat{u}) - 2m^2(m^2 + \hat{u})}{(m^2 - \hat{u})^2} - \frac{2}{3} \frac{m^2(\hat{s} - 4m^2)}{(m^2 - \hat{t})(m^2 - \hat{u})} \right. \\ \left. - \frac{6(m^2 - \hat{t})(m^2 - \hat{u}) + m^2(\hat{u} - \hat{t})}{\hat{s}(m^2 - \hat{t})} - \frac{6(m^2 - \hat{t})(m^2 - \hat{u}) + m^2(\hat{t} - \hat{u})}{\hat{s}(m^2 - \hat{u})} \right].$$

The corresponding lowest order QCD graphs are shown in Fig. (5.2).

The total normalization, $\sigma^{pA \rightarrow l\bar{l}} = B^2 \sigma^{pA \rightarrow H\bar{H}} = B^2 \sigma^{pA \rightarrow Q\bar{Q}}$, is obtained by integrating Eqs. (5.1) and (5.4) over the total phase space. Let us also define expressions for the double differential distribution,

$$\frac{d\tilde{\sigma}^{Q\bar{Q}}}{d^3\vec{p}_Q d^3\vec{p}_{\bar{Q}}} = \frac{1}{E_Q} \frac{1}{E_{\bar{Q}}} \left[\frac{1}{A} E_Q E_{\bar{Q}} \frac{d\sigma^{pA \rightarrow Q\bar{Q}+X}}{d^3\vec{p}_Q d^3\vec{p}_{\bar{Q}}} \right], \quad (5.11)$$

and the total cross section of $Q\bar{Q}$ production per nucleon,

$$\tilde{\sigma}^{Q\bar{Q}} = \int d^3\vec{p}_Q d^3\vec{p}_{\bar{Q}} \frac{d\tilde{\sigma}^{Q\bar{Q}}}{d^3\vec{p}_Q d^3\vec{p}_{\bar{Q}}} \\ = \int dp_T^2 dy_1 dy_2 \sum_{ij} x_1 f_i^p(x_1, Q^2) x_2 f_j^A(x_2, Q^2) \frac{d\hat{\sigma}^{ij \rightarrow Q\bar{Q}}}{d\hat{t}}, \quad (5.12)$$

where $x_{1,2} = m_T/\sqrt{s}(e^{\pm y_1} + e^{\pm y_2})$. The rapidities of the heavy quarks are $y_{1,2}$. The total $Q\bar{Q}$ cross sections per nucleon in pp and pA interactions are presented in Table (5.1).

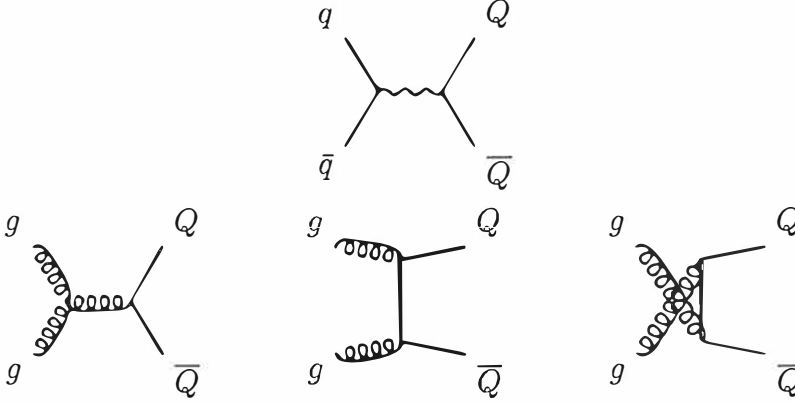


Figure 5.2: Lowest order QCD diagrams for $Q\bar{Q}$ production. Above: the $q\bar{q} \rightarrow Q\bar{Q}$. Below: $gg \rightarrow Q\bar{Q}$

	SPS ($A = 208$) [μb]	RHIC ($A = 197$) [μb]	LHC ($A = 208$) [μb]
$\tilde{\sigma}_{pp}^{c\bar{c}}$	1.188	143.7	6137
$\tilde{\sigma}_{pA}^{c\bar{c}}$	1.282	140.1	4826
$\tilde{\sigma}_{pp}^{b\bar{b}}$	1.674×10^{-5}	1.412	251.9
$\tilde{\sigma}_{pA}^{b\bar{b}}$	1.464×10^{-5}	1.513	226.7

Table 5.1: The total $Q\bar{Q}$ production cross sections per nucleon in pp and pA interactions.

5.2 Correlated v. uncorrelated pairs

In pA collision, along with correlated lepton pairs, i.e. leptons from same nucleon–nucleon subcollision, a number of uncorrelated pairs are produced. Since in general one would like to concentrate on correlated or uncorrelated pairs alone, separation of these different pairs is vital. In the Ref. [IV], we have also estimated the relative amounts of correlated and uncorrelated lepton pairs. To start with, we assume that all subprocess interactions are independent and the number of interaction can be described by a Poisson distribution. Let $\bar{N}_{Q\bar{Q}}$ be the average number of pp interactions per collision. We consider the impact parameter integrated $Q\bar{Q}$ cross section,

$$\sigma^{pA \rightarrow Q\bar{Q}+X} = \int d^2\mathbf{b} (1 - e^{-T_A(\mathbf{b})\tilde{\sigma}^{Q\bar{Q}}}) = \int d^2\mathbf{b} \sum_{N=1}^{\infty} \frac{\bar{N}_{Q\bar{Q}}^N(\mathbf{b}) e^{-\bar{N}_{Q\bar{Q}}(\mathbf{b})}}{N!}, \quad (5.13)$$

where \mathbf{b} is the impact parameter and the number of produced $Q\bar{Q}$ pairs is $\bar{N}_{Q\bar{Q}}(\mathbf{b}) = T_A(\mathbf{b})\tilde{\sigma}^{Q\bar{Q}}$. Multiplying it with the unit normalized $Q\bar{Q}$ distribu-

tion to power N and differentiating with respect to $d^3\vec{p}_Q d^3\vec{p}_{\bar{Q}}$ we get

$$\begin{aligned} \frac{d\sigma^{\text{pA} \rightarrow Q\bar{Q}+X}}{d^3\vec{p}_Q d^3\vec{p}_{\bar{Q}}} &= \int d^2\mathbf{b} \sum_{N=1}^{\infty} \frac{\bar{N}_{Q\bar{Q}}^N(\mathbf{b}) e^{-\bar{N}_{Q\bar{Q}}(\mathbf{b})}}{N!} \\ &\times \prod_{i=1}^N \left(\frac{1}{\bar{\sigma}^{Q\bar{Q}}} \int d^3\vec{p}_{Q_i} d^3\vec{p}_{\bar{Q}_i} \frac{d\bar{\sigma}^{Q\bar{Q}}}{d^3\vec{p}_{Q_i} d^3\vec{p}_{\bar{Q}_i}} \right) \left(\sum_{j,k=1}^N \delta^{(3)}(\vec{p}_Q - \vec{p}_{Q_j}) \delta^{(3)}(\vec{p}_{\bar{Q}} - \vec{p}_{\bar{Q}_k}) \right). \end{aligned} \quad (5.14)$$

The power N and the delta functions have been written as a product and a sum, respectively, in order to separate the subcollision to which they belong. This is indicated by indices j and k . For correlated pairs $j = k$, stating that Q and \bar{Q} originate from the same subcollision, whereas $j \neq k$ means that they come from different subcollisions.

Using the definition of the nuclear overlap function, $T_{AB}(\mathbf{b}) = \int ds T_A(s) \times T_B(\mathbf{b}-s)$ with $A = B$, and assuming Woods-Saxon distribution for the nuclear density, we get $\int d^2s T_A^2(s) = T_{AA}(\mathbf{0}) = A^2/(\pi R_A^2)$. Thus, for correlated pairs we find

$$\frac{d\sigma_{\text{corr}}^{\text{pA} \rightarrow Q\bar{Q}+X}}{d^3\vec{p}_Q d^3\vec{p}_{\bar{Q}}} = A \frac{d\bar{\sigma}^{Q\bar{Q}}}{d^3\vec{p}_Q d^3\vec{p}_{\bar{Q}}}, \quad (5.15)$$

while for uncorrelated pairs

$$\frac{d\sigma_{\text{uncorr}}^{\text{pA} \rightarrow Q\bar{Q}+X}}{d^3\vec{p}_Q d^3\vec{p}_{\bar{Q}}} = \frac{A^2}{\pi R_A^2} \frac{d\bar{\sigma}^{Q\bar{Q}}}{d^3\vec{p}_Q} \frac{d\bar{\sigma}^{Q\bar{Q}}}{d^3\vec{p}_{\bar{Q}}}. \quad (5.16)$$

As seen in Eq. (5.16), the cross section of uncorrelated pairs is a product of two independent single quark cross sections. This fact can be utilized to study the ratio of cross sections of uncorrelated lepton pairs from pA and pp collisions. The uncorrelated ratio would probe the square of the nuclear modifications, $(R_g^A)^2$, instead of R_g^A as the correlated ratio does.

5.3 Numerical calculations

We calculated the lepton pair cross sections by generating numerically lepton pairs in proton-nucleus collision using a Monte Carlo method. For simplicity we have assumed a nucleus to consist of A protons. As the $gg \rightarrow Q\bar{Q}$ is the dominant process for heavy quark production, and as the gluon parton distribution is the same for protons and neutrons, this assumption will not significantly affect on the results. We used MRST98 LO (central gluon) parton distribution functions [11] from PDFLIB [57] along with EKS98 [II] nuclear modifications. Factorization scale was chosen to be $Q^2 = 4m_T^2$ for $c\bar{c}$ and $Q^2 = m_T^2$ for $b\bar{b}$.

The c quark fragments into D^+ , D^0 and D_s mesons with relative respective weight 1:1:0.3 [56]. However, in this study we neglected D_s mesons, which should not affect significantly the results. The other quarks were fragmented similarly: $\bar{c} \rightarrow D^-$ and \bar{D}^0 ; $b \rightarrow B^+$ and \bar{B}^0 ; and $\bar{b} \rightarrow B^-$ and B^0 .

We used JETSET/PYTHIA [56] subroutines to describe the decay of mesons. To obtain statistically adequate results we created 2×10^6 $Q\bar{Q}$ pairs, and let each pair separately fragment and decay 10^3 times. Factor of two originates from the fact that the uncorrelated lepton pairs were formed from two different $Q\bar{Q}$ pairs.

We then searched all the $e^\pm e^\mp$, $\mu^\pm \mu^\mp$ and $e^\pm \mu^\mp$ pairs, and binned them according to their mass and rapidity. We also calculated the average $\langle x_1 \rangle$, $\langle x_2 \rangle$ and $\langle Q \rangle$, as well as the average of their squares, for each $(y_{i\bar{i}}, M_{i\bar{i}})$ bin.

The pp and pA results were calculated for SPS ($\sqrt{s}=17.3$ GeV), RHIC ($\sqrt{s}=200$ GeV) and LHC ($\sqrt{s}=5500$ GeV), using the same center of mass energies as in AA collisions to probe the same x values in all collisions. At the SPS and LHC, we assume a Pb ($A=208$) target and an Au ($A=197$) target at RHIC.

Detector based rapidity cuts were imposed, but generally we did not attempt to simulate the features of different detectors. For instance azimuthal angle cuts as well as minimum energy cuts were not included.

5.4 Ratio of lepton pair cross sections

The ratio of cross sections of lepton pairs,

$$r_\sigma \equiv \frac{d\sigma^{\text{pA}}/dM}{d\sigma^{\text{pp}}/dM}, \quad (5.17)$$

for correlated $e^\pm e^\mp$ and $\mu^\pm \mu^\mp$ pairs from $D\bar{D}$ and $B\bar{B}$ decays in pA and pp collisions is shown in Fig. (5.3) at the SPS, RHIC and LHC energies (solid curves). The cross sections are integrated over the pair rapidity. These ratios are compared to the nuclear gluon modifications, $R_g(x, Q)$ at $x = \langle x_2 \rangle$, and both at $Q = \langle Q \rangle$ (dashed curves) and $Q = \sqrt{\langle Q^2 \rangle}$ (dotted-dashed curves). The Fig. (5.3) shows that the ratio R_g^A indeed follows closely the ratio of cross sections r_σ . The higher the energy, the better is the agreement. The difference between r_σ and R_g^A is caused partly because some of the $Q\bar{Q}$ pairs are produced through the $q\bar{q} \rightarrow Q\bar{Q}$ channel, and partly by the phase space integration, as explained in Ref. [IV].

Similarly, the ratios of uncorrelated cross sections were compared to $(R_g^A)^2$. The behaviour is similar as in the correlated case, now only the

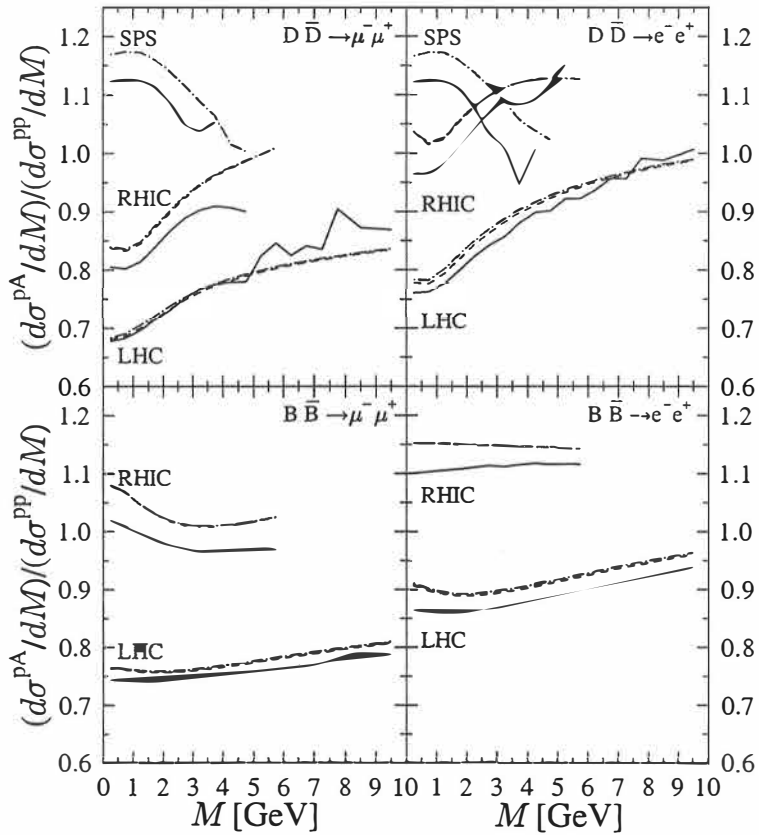


Figure 5.3: The ratio of $e^\pm e^\mp$ and $\mu^\pm \mu^\mp$ pair cross sections from correlated $D\bar{D}$ and $B\bar{B}$ decays in pA and pp collisions, r_σ , at SPS, RHIC and LHC energies (solid curves). The nuclear gluon distribution, $R_g^A(x_2, Q)$, at $\langle x_2 \rangle$ and $\langle Q \rangle$ ($\sqrt{\langle Q^2 \rangle}$) of each $M_{l\bar{l}}$ bin is indicated by the dashed (dotted-dashed) curves.

difference between r_σ^{uncorr} and $(R_g^A)^2$ is slightly larger. This is due to the increased phase space effects as the integration over the rapidity of one of the leptons allows a larger phase space for the other one.

The results are encouraging: measurements with sufficient accuracy could be used to pin down the behaviour of nuclear gluon distributions at different regions of momentum fraction x .

Chapter 6

Conclusions

We have studied the nuclear effects of parton distributions, with our main goal to obtain expressions for the nuclear modifications for the parton distributions, the ratios of nuclear v. free parton distributions. We have also studied ways to find constraints for sea quark and gluon distributions. As comparison to experiments we studied whether the observed Q^2 evolution of $F_2^{\text{Sn}}/F_2^{\text{C}}$ can be described in terms of DGLAP evolution.

We based our analysis on the experimental data only and did not use any specific model of nuclear effects. Using data from deep inelastic lepton-nucleus scattering and Drell-Yan experiments we have produced a scale dependent parametrization of nuclear modifications of parton distributions. Using the produced parametrization we have calculated the ratio of structure functions of tin v. carbon, $F_2^{\text{Sn}}/F_2^{\text{C}}$. Our calculations are in good agreement with the corresponding NMC data, as shown Fig. (3.4). Although the higher twist, $\sim 1/Q^2$, effects are interesting in the low Q^2 region, they do not seem to play a significant role in the observed scale evolution and the leading order DGLAP analysis is sufficient to explain the observed phenomena, at least in the region $x \gtrsim 0.01$ and $Q^2 > 2.25 \text{ GeV}^2$.

As additional constraints for the nuclear modifications are still needed, we have further studied the EMC region of sea distributions. By assuming several different scenarios for the behaviour of sea distributions, we have shown that the assumed EMC effect of sea quarks, if really there, could be observed in the Drell-Yan process. Although the effect turns out to be small in pA collisions, it could be detected for example in the Pb-Pb collisions at SPS with $E_{\text{lab}} = 158 \text{ AGeV}$.

In attempt to find restrictions for the nuclear gluon distributions, their effect on the ratio of lepton pair cross sections in pA and pp collisions was studied. The ratio of cross sections of lepton pairs reflects quite well the nuclear gluon modifications and can be used to probe them, assuming that

the experimental measurements can be done with sufficient accuracy. Several such measurements have been proposed. The NA60 experiment at the SPS [59], the PHENIX detector at RHIC [60] and the ALICE detector at LHC [61] provide all a possibility to measure nuclear effects at different \sqrt{s} and x regions. At NA60, a 20 % antishadowing in R_g^A induce a 10 % enhancement in the ratio of cross sections. The measurements within this accuracy would fix the nuclear gluon distribution at region $0.17 \lesssim x \lesssim 0.4$. At higher energies the gg channel becomes more dominant and the R_g^A follows the ratio of cross sections more closely. At RHIC, the PHENIX detector could be used to measure the heavy quark production with x values as low as 3×10^{-3} . The ALICE detector at the LHC goes even lower, down to 3×10^{-5} .

Generally it appears that this study explains well the scale dependent behaviour of parton distributions in nuclei. However, plenty of future work still remains. A procedure in which new data could be automatically included would be very useful. Also a proper χ^2 minimization should be included into the determination of the initial effects $R_i^A(x, Q_0^2)$. The next-to-leading order calculations would provide a more consistent analysis, although we do not expect the NLO effects affect very much the ratio of parton distributions. Also the higher twist effects both in evolution and in multiple scatterings require further analysis. The parametrization method could also be streamlined: instead of parametrizing the ratio F_2^A/F_2^D at the initial scale Q_0^2 , one could parametrize directly the ratios R_V^A and R_S^A at this scale.

In this study we have not utilized the neutrino data for structure functions F_2 and F_3 , because of their limited statistic [62]. The neutrino data with increased statistics and mass number systematics could be taken into account in the analysis in the future.

Appendix A

EKS98 parametrization

In the Ref. [II] the nuclear parton distributions have been parametrized¹ for each parton flavour ($u_v, d_v, \bar{u}, \bar{d}, s, c, b, g$) and for 8 values of A (4, 9, 12, 27, 40, 56, 117, 208) at 180 values of $10^{-6} < x < 1$ and 69 values of $2.25 \text{ GeV}^2 < Q^2 < 10^4 \text{ GeV}^2$. This makes 794880 numbers in total. For practical purposes we have introduced a further parametrization of the nuclear modifications by parametrizing each of the above variable separately using MINUIT Fortran code [58] for χ^2 minimization.

The outline of the parametrization is following: First, the Q^2 dependence was parametrized using a function

$$R^k(x, Q^2, A) = R_0 + p_1^k(x, A)z + p_2^k(x, A)z^2 + p_3^k(x, A)\sqrt{z}, \quad (\text{A.1})$$

with the initial conditions $R_0 \equiv R^k(x, Q_1^2, A)$ and $z \equiv \log(Q^2/Q_1^2)$. Scale Q_1^2 is the minimum Q^2 for each parton: for light quarks and gluons it is Q_0^2 , and for c and b it is the mass threshold:

$$Q_1^2 = Q_0^2 = 2.25 \text{ GeV}^2 \quad \text{for } u_v, d_v, \bar{u}, \bar{d}, s \text{ and } g, \quad (\text{A.2})$$

$$Q_1^2 = 2.54958 \text{ GeV}^2 \quad \text{for } c, \quad (\text{A.3})$$

$$Q_1^2 = 21.3474 \text{ GeV}^2 \quad \text{for } b. \quad (\text{A.4})$$

The x dependence of the coefficient functions ($p_1^k(x, A)$, $p_2^k(x, A)$ and $p_3^k(x, A)$) was then fixed using a piecewise construction with 10 functions:

$$p_i^k(x, A) = \begin{cases} p_{i0}(A) + k_1^i(A)z' + k_2^i(A)z'^2 + k_3^i(A)x' + k_4^i(A)x'^2 & \text{if } x < x_{116} \\ C + k_5^i(A)\bar{x} + k_6^i(A)\bar{x}^2 + k_7^i(A)\bar{x}^3 + k_8^i(A)\bar{x}^E + k_9^i(A)\bar{z} & \text{if } x > x_{116}, \end{cases} \quad (\text{A.5})$$

¹The numerical work for the parametrization is done mainly by C.A. Salgado.

where $z' = \ln(x/x_0)$, $\bar{z} = \ln(x/x_{116})$, $x' = x - x_0$ and $\bar{x} = x - x_{116}$. The parameter C is fixed by the continuity of p_i at $x = x_{116}$, where x_{116} is the 116th element in the x grid. In addition, $x_0 \equiv 10^{-6}$, $p_{i0}(A) \equiv p_i(x_0, A)$ and

$$E = \begin{cases} 19 & \text{for } p_1 \text{ and } p_2 \\ 27 & \text{for } p_3. \end{cases} \quad (\text{A.6})$$

Next, the A dependence of each of the 10 previous coefficients (including p_{i0}) was parametrized using a function

$$k_i^j = k_i^j(A=4) + a_{i1}^j \bar{z} + a_{i2}^j \bar{z}^2 \quad (\text{A.7})$$

with $\bar{z} = \ln(A/4)$.

As a result, the parametrization is described with $3 \times 10 \times 8 \times 3 = 720$ numbers plus the initial conditions for R^k of each parton flavour at $Q^2 = Q_1^2$ as a function of x and A .

Finally, the A dependence of initial conditions R^k are also parametrized using a similar functional form as in (A.7):

$$R^k(x, Q_1^2, A) = R^k(x, Q_1^2, 4) + b_1^k \bar{z} + b_2^k \bar{z}^2 \quad (\text{A.8})$$

where, as before, $\bar{z} = \ln(A/4)$. In this manner the initial conditions can be described with $180 \times 3 \times 8$ numbers.

As the ratios R_i^A are approximately set-independent [II], the absolute parton distributions of protons in a nucleus A with Z protons and $(A - Z)$ neutrons can be obtained simply by multiplying the parton distributions f_i^p of any modern lowest order set by parametrization R_i^A .

$$f_i^{p/A}(x, Q^2) = R_i^A(x, Q^2) f_i^p(x, Q^2). \quad (\text{A.9})$$

Assuming the isospin symmetry, the corresponding distributions can also be obtained for the bound neutrons.

Based on this parametrization, a Fortran code named as EKS98 [II] was created and released for public use. It provides nuclear modifications $R_i^A(x, Q^2)$ for $10^{-6} \leq x \leq 1$, $2.25 \text{ GeV}^2 \leq Q^2 \leq 10^4 \text{ GeV}^2$ and $2 \leq A$ for each parton flavour $i = (g, u_v, d_v, \bar{u}, \bar{d}, s, c, b)$. This code has also been included in the recent version of the CERN PDFLIB library [57].

Bibliography

- [I] K.J. Eskola, V.J. Kolhinen and P.V. Ruuskanen, Nucl. Phys. **B535** (1998) 351.
- [II] K.J. Eskola, V.J. Kolhinen and C.A. Salgado, Eur. Phys. J. **C9** (1999) 61.
- [III] K.J. Eskola, V.J. Kolhinen, C.A. Salgado and R.L. Thews, JYFL-4/00, LPT Orsay 00-73, hep-ph/0009251, submitted to Eur. Phys. J. C.
- [IV] K.J. Eskola, V.J. Kolhinen and R. Vogt, JYFL-6/01, hep-ph/0104124, accepted to Nucl. Phys. A.

- [1] F. Halzen, A.D. Martin, *Quarks and Leptons: An Introductory Course in Modern Particle Physics*, John Wiley & Sons, Inc 1984.
- [2] R.D. Field, *Applications of Perturbative QCD*, Addison-Wesley Publishing Company, 1989, 1995.
- [3] K.J. Eskola, *Deep inelastic scattering, Drell-Yan and parton distributions*, Lectures on the 7th International Summer School, Jyväskylä, Finland, 1997.
- [4] M. Abramowitz and I.A. Stegun (*Ed.*), *Handbook of Mathematical Functions*, 9th edition, Dover Publications Inc, 1970.
- [5] G. Altarelli, R.K. Ellis, G. Martinelli, Nucl. Phys. **B157** (1979) 461.
- [6] R.K. Ellis and W.J. Stirling, *QCD and collider physics*, FERMILAB-Conf-90/164-T, August 14, 1990.
- [7] S. Gavin, R. Kauffman, S. Gupta, P. V. Ruuskanen, D. K. Srivastava and R. L. Thews, Int. J. Mod. Phys. **A10** (1995) 2961.
- [8] P.J. Sutton, A.D. Martin, R.G. Roberts and W.J. Stirling, Phys. Rev. **D45** (1992) 2349.

- [9] J. Kubar, M. Le Bellac, J.L. Meunier and G. Plaut, Nucl. Phys. **B175** (1980) 251.
- [10] P.J. Rijken and W.L. van Neerven, Phys. Rev. **D51** (1995) 44.
- [11] A.D. Martin, R.G. Roberts, W.J. Stirling, R.S. Thorne, Eur. Phys. J. **C4** (1998) 463.
- [12] H. L. Lai *et al.*, Phys. Rev. **D55** (1997) 1280.
- [13] M. Glück, E. Reya and A. Vogt, Z. Phys. **C53** (1992) 127.
- [14] M. Glück, E. Reya and A. Vogt, Eur. Phys. J. **C5** (1998) 461.
- [15] EMC collaboration, J.J. Aubert *et al.*, Phys. Lett. **B123** (1983) 275; A. Bodek *et al.*, Phys. Rev. Lett. **50** (1983) 1431; **51** (1983) 534.
- [16] NMC collaboration, M. Arneodo *et al.*, Nucl. Phys. **B481** (1996) 23.
- [17] NMC collaboration, P. Amaudruz *et al.*, Nucl. Phys. **B441** (1995) 3.
- [18] NMC collaboration, M. Arneodo *et al.*, Nucl. Phys. **B441** (1995) 12.
- [19] NMC collaboration, M. Arneodo *et al.*, Nucl. Phys. **B481** (1996) 3.
- [20] J. Gomez *et al.*, Phys. Rev. **D49** (1994) 4348.
- [21] E665 collaboration, M.R. Adams *et al.*, Phys. Rev. Lett. **68** (1992) 3266.
- [22] E665 collaboration, M.R. Adams *et al.*, Z. Phys. **C67** (1995) 403.
- [23] H1 Collaboration, I. Abt *et al.*, Nucl. Phys. **B407** (1993) 515; T. Ahmed *et al.*, Nucl. Phys. **B439** (1995) 471; ZEUS Collaboration, M. Derrick *et al.*, Phys. Lett. **B316** (1993) 412; Z. Phys. **C65** (1995) 379.
- [24] H1 Collaboration, S. Aid *et al.*, Nucl. Phys. **B470** (1996) 3.
- [25] D.M. Alde *et al.*, Phys. Rev. Lett. **64** (1990) 2479.
- [26] E866 Collaboration, M.A. Vasiliev *et al.*, Phys. Rev. Lett. **83** (1999) 2304.
- [27] L.V. Gribov, E.M. Levin and M.G. Ryskin, Nucl. Phys. **B188** (1981) 555; Phys. Rep. **100** (1983) 1.
- [28] A.H. Mueller and J. Qiu, Nucl. Phys. **B268** (1986) 427.

- [29] SLAC E140 Collaboration, S. Dasu *et al.*, Phys. Rev. Lett. 61 (1988) 1061.
- [30] SLAC E140 Collaboration, L. Whitlow *et al.*, Phys. Lett. **B250** (1990) 193.
- [31] NA37/NMC, P. Amaudruz *et al.*, Phys. Lett. **B294** (1992) 120.
- [32] M. Arneodo, Phys. Rep. **240** (1994) 301.
- [33] NA51 Collaboration, A. Baldit *et al.*, Phys. Lett. **B332** (1994) 244.
- [34] L.L. Frankfurt, M.I. Strikman and S. Liuti, Phys. Rev. Lett. **65** (1990) 1725.
- [35] Jianwei Qiu, Nucl. Phys. **B291** (1987) 746.
- [36] K.J. Eskola, Nucl. Phys. **B400** (1993) 240.
- [37] N.N. Nikolaev and V.I. Zakharov, Phys. Lett. **B55** (1975) 397; V.I. Zakharov and N.N. Nikolaev, Sov. J. Nucl. Phys. 21 (1975) 227.
- [38] G. Grammer and J.D. Sullivan, *Nuclear shadowing of electromagnetic processes in Electromagnetic Interactions of Hardons*, Eds. A. Donnachie and G. Shaw, Vol 2., Plenum Press, New York, 1978, p. 195; A. Donnachie and G. Shaw, *Generalized vector dominance in Electromagnetic Interactions of Hardons*, Eds. A. Donnachie and G. Shaw, Vol 2., Plenum Press, New York, 1978, p. 169.
- [39] T.H. Bauer *et al.*, Rev. Mod. Phys. 50 (1978) 261; erratum: 51 (1979) 407.
- [40] P. Castorina and A. Donnachie, Phys. Lett. B 215 (1988) 508; Z. Phys. **C45** (1989) 141.
- [41] G. Preparata and P.G. Ratcliffe, Phys. Lett **B276** (1992) 219; preprint MITH 91/13, University of Milano (1991).
- [42] J. Kwieciński and B. Badelek, Phys. Lett. **B208** (1988) 508.
- [43] J. Kwieciński, Z. Phys. **C45**(1990) 461.
- [44] G. Altarelli, G. Parisi, Nucl. Phys. **B126** (1977) 298.
- [45] V.N. Gribov and L.N. Lipatov, Sov. Nucl. Phys. **15** (1972) 438, 675.

- [46] Yu. Dokshitzer, Sov Phys. JETP **46** (1977) 641.
- [47] T. Gousset and H.J. Pirner, Phys. Lett. **B375** (1996) 349.
- [48] K. Prytz, Phys. Lett. **B311** (1993) 286.
- [49] S. Gavin, P.L. McGaughey, P.V. Ruuskanen and R. Vogt, Phys. Rev. **C54** (1996) 2606.
- [50] Z. Lin and M. Gyulassy, Nucl. Phys. **A610** (1996) 476.
- [51] B.L. Combridge, Nucl. Phys. **B151** (1979) 429.
- [52] C. Peterson, D. Schlatter, I. Schmitt, and P.M. Zerwas. Phys. Rev. **D27** (1983) 105.
- [53] B. Badelek and J. Kwieciński, Phys. Rev. **D50** (1994) 4; Nucl. Phys. **B370** (1992) 278.
- [54] K. J. Eskola, K. Kajantie, P. V. Ruuskanen and K. Tuominen, Nucl. Phys. **B570** (2000) 379.
- [55] K. J. Eskola, P. V. Ruuskanen, S. S. Räsänen and K. Tuominen, hep-ph/0104010.
- [56] T. Sjöstrand, Computer Physics Comm. 82 (1994) 74.
- [57] H. Plochow-Besch, Comp. Phys. Comm. 75 (1993) 396; Int. J. Mod. Phys. **A10** (1995) 2901; "PDFLIB: Proton, Pion and Photon Parton Density Functions, Parton Density Functions of the Nucleus, and α_s ", Users's Manual - Version 8.04, W5051 PDFLIB 2000.04.17 CERN-ETT/TT.
- [58] F. James, "MINUIT: Function minimalization and error analysis", Reference Manual, version 94.1, CERN Program Library Long Writeup D506.
- [59] A. Baldit *et al.* (NA60 Collab.), Proposal SPSC/P316, March 2000; <http://na60.web.cern.ch/NA60>.
- [60] D.P. Morrison *et al.* (PHENIX Collab.), Nucl. Phys. **A638** (1998) 565c.
- [61] ALICE Collaboration, Technical Proposal, CERN/LHCC 95-71, ALICE Collaboration, Addendum to the Letter of Intent, CERN/LHCC 95-24, ALICE Collaboration, Addendum to ALICE Proposal, CERN/LHCC 99-13.

- [62] BEBC Collaboration, J. Guy *et al.*, Phys. Lett. **B229** (1989) 421, BEBC WA59 Collaboration, P.P. Allport *et al.*, Phys. Lett. **B232** (1989) 417.